DNA sequence-directed cooperation between nucleoid-associated proteins

Japaridze, Aleksandre; Yang, Wayne; Dekker, Cees; Nasser, William; Muskhelishvili, Georgi

DOI
10.1016/j.isci.2021.102408

Publication date
2021

Document Version
Final published version

Published in
iScience

iScience

CellPress
OPEN ACCESS

Article

DNA sequence-directed cooperation between nucleoid-associated proteins

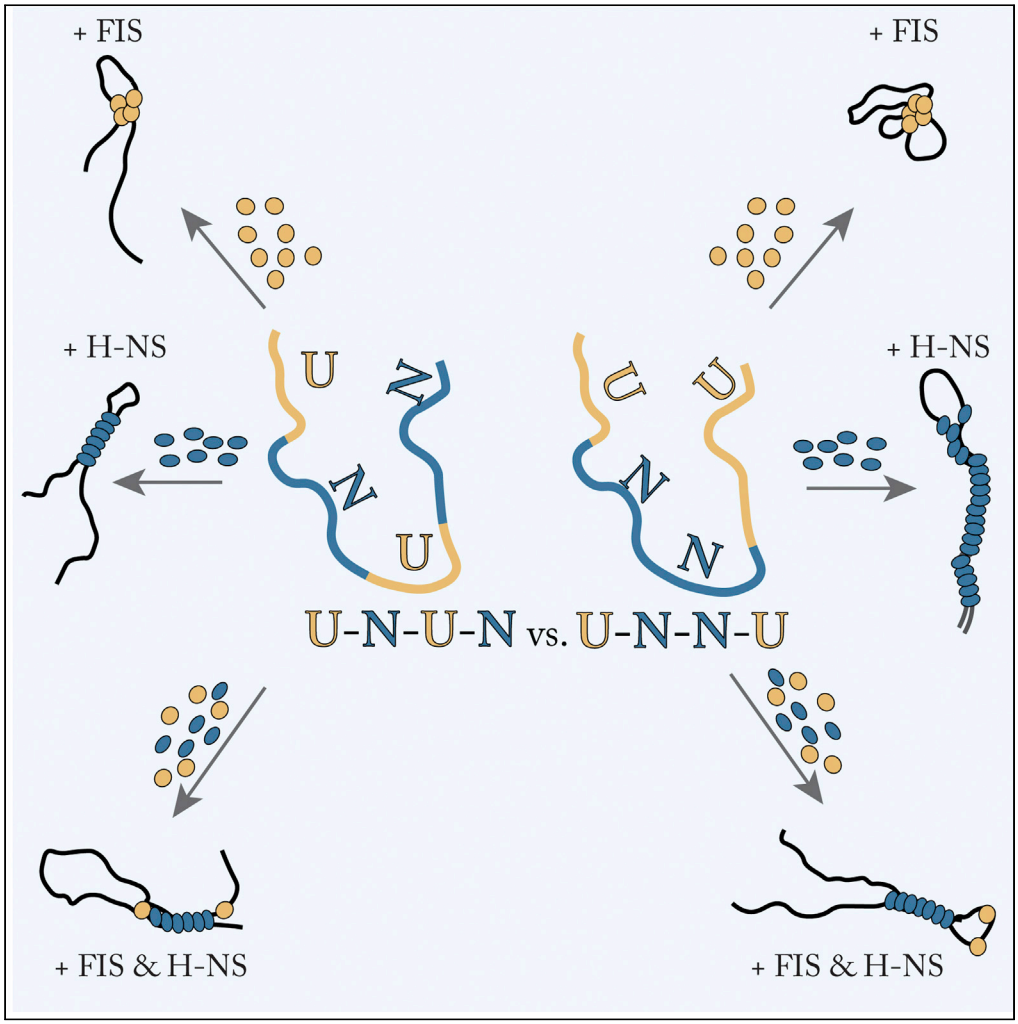

Aleksandre Japaridze, Wayne Yang, Cees Dekker, William Nasser, Georgi Muskhelishvili

a.japaridze@tudelft.nl

Highlights

The location of protein binding sites along DNA is important for 3D organization

FIS protein forms DNA loops while H-NS forms compact DNA plectonemes

FIS DNA loops inhibit H-NS from spreading over the DNA

FIS and H-NS competition creates regions of 'open' and 'closed' DNA

Japaridze et al., iScience *24*, 102408
May 21, 2021
https://doi.org/10.1016/j.isci.2021.102408

iScience

CellPress
OPEN ACCESS

Article

DNA sequence-directed cooperation between nucleoid-associated proteins

Aleksandre Japaridze,[1,4,*] Wayne Yang,[1] Cees Dekker,[1] William Nasser,[2] and Georgi Muskhelishvili[3]

SUMMARY

Nucleoid-associated proteins (NAPs) are a class of highly abundant DNA-binding proteins in bacteria and archaea. While both the composition and relative abundance of the NAPs change during the bacterial growth cycle, surprisingly little is known about their crosstalk in mutually binding and stabilizing higher-order nucleoprotein complexes in the bacterial chromosome. Here, we use atomic force microscopy and solid-state nanopores to investigate long-range nucleoprotein structures formed by the binding of two major NAPs, FIS and H-NS, to DNA molecules with distinct binding site arrangements. We find that spatial organization of the protein binding sites can govern the higher-order architecture of the nucleoprotein complexes. Based on sequence arrangement the complexes differed in their global shape and compaction as well as the extent of FIS and H-NS binding. Our observations highlight the important role the DNA sequence plays in driving structural differentiation within the bacterial chromosome.

INTRODUCTION

Nucleoid-associated proteins (NAPs) represent a small class of highly abundant DNA architectural proteins involved in shaping the bacterial chromatin and in regulating the gene expression in prokaryotes and archaea (Dame et al., 2020; Dillon and Dorman, 2010; Driessen and Dame, 2011; Luijsterburg et al., 2006; Travers and Muskhelishvili, 2005). During the bacterial growth cycle, these proteins are expressed in a growth-phase-dependent manner to coordinate the chromosome structure with the metabolic state (Azam et al., 1999; Sobetzko et al., 2012; Sonnenschein et al., 2011; Travers and Muskhelishvili, 2020). NAPs bind DNA with varying affinities from nanomolar to micromolar concentrations and affect the gene expression by acting as bona fide transcription factors as well as so-called "topological homeostats" (Muskhelishvili and Travers, 2003; Travers et al., 2001). The regulation of genomic transcription by NAPs is closely coupled with their propensity to modulate the availability of free or "unconstrained" DNA superhelicity, as NAPs constrain the DNA acting both as supercoil repositories and topological barriers to supercoil diffusion (Berger et al., 2016; Dages et al., 2020; Hardy and Cozzarelli, 2005; Hatfield and Benham, 2002; Muskhelishvili and Travers, 2003).

Factor for Inversion Stimulation (FIS) protein is the most abundant NAP during the exponential growth phase in *Escherichia coli*, while its concentration quickly drops to undetectable levels upon the transition of cells to stationary phase (Azam et al., 1999; Ball et al., 1992; Ninnemann et al., 1992). FIS has a global nucleoid-structuring function (Fisher et al., 2013; HadizadehYazdi et al., 2012; Wu et al., 2019a, 2019b) as well as local accessory roles in the assembly of synaptic complexes by site-specific recombinases (Ball and Johnson, 1991; Mertens et al., 1988) and transcription-initiation complexes at various promoters, including the exceptionally strong RNA (rRNA and tRNA) promoters (Bokal et al., 1995; Lazarus and Travers, 1993). The latter are characterized by upstream activating sequences (UAS) containing multiple FIS-binding sites that are arranged in a helical register (Hirvonen et al., 2001). FIS is a helix-turn-helix (HTH) DNA-bending protein (Stella et al., 2010) which upon binding at the phased sites in UAS forms a coherently bent DNA loop that associates with RNA polymerase (Maurer et al., 2006). In general, FIS nucleoprotein complexes form loops and stabilize branches in supercoiled DNA (Japaridze et al., 2017a; Schneider et al., 2001; Skoko et al., 2006; Travers et al., 2001).

In contrast to FIS, the histone-like nucleoid-structuring (H-NS) protein is an NAP expressed throughout the entire bacterial growth cycle (Azam et al., 1999), slightly increasing in concentration toward the later growth stages. While overproduction of H-NS *in vivo* is lethal for the cell (Spurio et al., 1992), the deletion of the

[1]Department of Bionanoscience, Kavli Institute of Nanoscience Delft, Delft University of Technology, Van der Maasweg 9, 2629 HZ Delft, The Netherlands

[2]Université de Lyon, INSA Lyon, Université Claude Bernard Lyon 1, CNRS UMR5240, Laboratoire de Microbiologie, Adaptation et Pathogénie, 69621 Villeurbanne, France

[3]School of Natural Sciences, Agricultural University of Georgia, Davit Aghmashenebeli Alley 240, 0159 Tbilisi, Georgia

[4]Lead contact

*Correspondence: a.japaridze@tudelft.nl

https://doi.org/10.1016/j.isci.2021.102408

H-NS gene does not result in large-scale restructuring of the nucleoid (Brunetti et al., 2001; Lioy et al., 2018; Wu et al., 2019a). H-NS is a DNA-bridging protein that binds preferentially to AT-rich DNA sequences (Dorman, 2007; Grainger et al., 2006; Lang et al., 2007; Lucchini et al., 2006; Navarre et al., 2006), in part mediated by an A-T hook motif that interacts with the DNA minor groove (Badaut et al., 2002; Gordon et al., 2011). It was shown that H-NS can bridge two DNA helices within a rigid filament (Dame et al., 2000; Schneider et al., 2001), trapping RNA polymerase (Dame et al., 2001; Schröder and Wagner, 2000). It is assumed that binding of H-NS nucleates at high-affinity sites and subsequently spreads along the DNA strands, leading to gene silencing (Bouffartigues et al., 2007; Kahramanoglou et al., 2011; Shin et al., 2012). While H-NS can polymerize on a single DNA duplex, resulting in its stiffening (Liu et al., 2010), it is the DNA-bridging mode facilitated by Mg^{2+} ions that has been primarily implicated in transcriptional repression (Kotlajich et al., 2015; Lim et al., 2012; van der Valk et al., 2017).

While the structural role of FIS, H-NS, and other DNA-binding NAPs has been intensively studied (Dame et al., 2000; Fisher et al., 2013; Hadizadeh Yazdi et al., 2012; Maurer et al., 2006; Schneider et al., 2001; Wu et al., 2019a, 2019b), surprisingly little is known about putative cooperative binding effects and the architecture of the ensuing long-range DNA structures. From NAP expression patterns (Azam et al., 1999) it is clear that distinct combinations of these proteins interact with the genomic DNA during the different stages of the cell cycle (Travers and Muskhelishvili, 2020). Indeed, exploration of their cooperative binding effects appears indispensable for understanding the growth phase-dependent gene regulation. Interestingly, previous studies using atomic force microscopy (AFM) showed that cooperative binding of various combinations of NAPs to the linear phage λ-DNA led to regular structures that were quite distinct from those observed with individual proteins (Maurer et al., 2009), while on binding to large supercoiled molecules, NAPs did phase separate, forming domain-like regions (Japaridze et al., 2017a). Resolving specific higher-order structures formed by cooperative binding of NAPs is challenging, but it can be achieved by using model DNA sequences that contain a few high-affinity binding sites that facilitate the nucleation of long-range nucleoprotein complexes.

Here, we explore whether the binding of a combination of two major bacterial NAPs, FIS and H-NS, leads to the emergence of distinct nucleoprotein structures that are more than the mere sum of those formed by the individual NAPs. To address this question, we employed DNA sequences with various arrangements of FIS and H-NS binding sites and studied the resulting higher-order nucleoprotein complexes using AFM and nanopore experiments. We find that sequential organization of the binding sites directs the assembly of peculiar nanometer-sized hairpin-like DNA architectures by FIS and H-NS, which are not observed with either FIS or H-NS alone. Furthermore, we find that FIS and H-NS self-organize to separate domains along the DNA molecules when both proteins are present. Our results exemplify the type of structural rearrangements that local DNA regions can undergo during bacterial growth cycle, highlighting the crucial role of the DNA sequence in this process.

RESULTS

DNA sequence directs cooperative binding of FIS and H-NS

To study the combined effects of native FIS and H-NS proteins (Lautier and Nasser, 2007; Nasser and Reverchon, 2002) binding to DNA, we used two ~4kb plasmids of ~1300nm length that differed in the sequence arrangement of the NAP-binding sites. In one construct, we arranged an FIS-binding sequence UAS and an H-NS-binding sequence NRE in a head-to-tail (HT) fashion (HT: UAS-NRE-UAS-NRE). Here, UAS is the upstream activating sequence of tyrosyl-tRNA gene promoter (*tyrT* UAS) (Lamond and Travers, 1983) and NRE is the negative regulatory element of proV gene (*proV* NRE) from an osmoregulatory operon (Gowrishankar, 1985). In the second construct, the same NAP-binding sequences were arranged in a head-to-head (HH) fashion (HH: UAS-NRE-NRE-UAS). These sequences were inserted into a 2.9kb plasmid backbone devoid of any strong FIS or H-NS binding sites (Japaridze et al., 2017b) (Figures 1A and 1E, see transparent methods). The 397bp-long *tyrT* UAS region contained three specific FIS binding sites (with K_d values ranging between 7.5 nM and 60 nM) arranged in a helical register (Lazarus and Travers, 1993), while the 264 bp long *proV* NRE contained two high-affinity H-NS sites (K_d values between 15 nM and 25 nM) separated by about 10 helical turns and many low affinity sites (Bouffartigues et al., 2007). The constructs with HT and HH arrangements have been described in detail in a previous study (Japaridze et al., 2017b), which showed that the binding of H-NS to various arrangements of high-affinity binding sites led to the formation of distinct long-range plectonemically coiled structures. Increasing concentrations of bound H-NS resulted in gradual shortening of the DNA contour length, indicating that H-NS protein upon binding was braiding

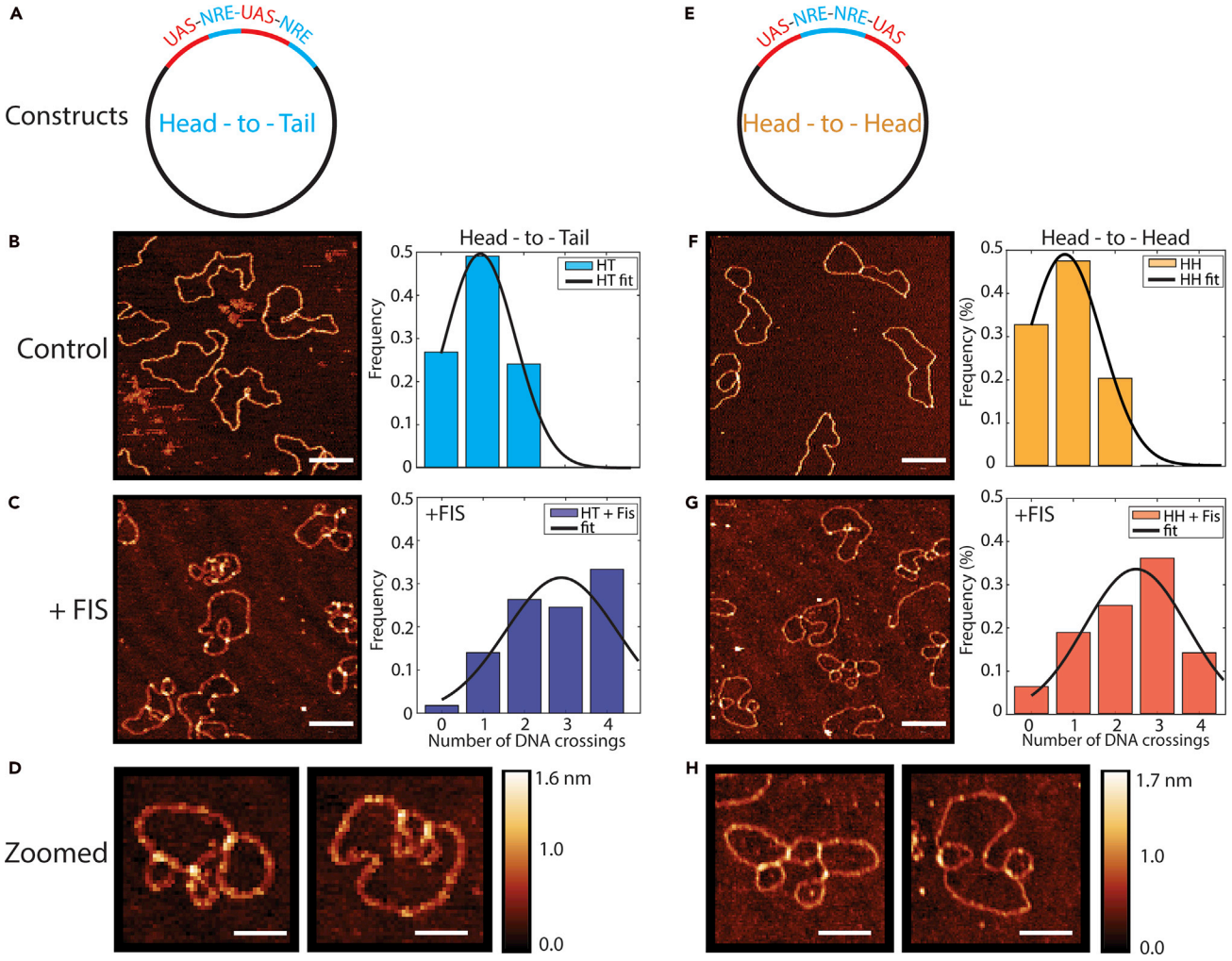

Figure 1. AFM images of FIS nucleoprotein complexes formed on circular nicked DNA constructs

Schematic depiction of (A) the head-to-tail (HT) and (E) head-to-head (HH) circular constructs.

AFM images of (B) control HT and (F) control HH plasmids deposited on mica without proteins with the respective number of DNA loops (right panels in B and F).

Upon the addition of FIS protein (FIS:bp ratio = 0.0026) to (C) the HT plasmid as well as to the (G) HH plasmid, the number of DNA loops increased about threefold. Solid lines denote Gaussian fits. Scale bars 200nm. Zoomed in AFM images of FIS looped structures for (D) HT and (H) HH plasmids . Scale bars 100nm.

the DNA into a twisted structure rather than just bridging the duplexes (which would not result in a reduction of the contour length). These nucleoprotein structures differed in their shape, compaction, and capacity to constrain DNA supercoils.

First, we investigated nucleoprotein structures formed by the binding of the native FIS protein to these constructs. We incubated FIS with either the nicked circular HT or HH plasmid and subsequently imaged by AFM in air (see transparent methods). We found that binding of the protein induced global changes in the shapes of both DNA constructs. FIS stabilized DNA crossovers and loops (Figures 1B–1D and 1F–1H). This is in sharp contrast to the plectonemic DNA structures stabilized by H-NS (Japaridze et al., 2017b) (see also Figure S1). Upon deposition on the surface, naked plasmids displayed, on average, a single DNA crossing (Figures 1B and 1F, average number of crossings is 1.0 for HT (N = 108) and 0.9 for HH (N = 129)). Upon co-incubation with FIS, however, the number of loops increased almost three times to 2.8 for HT (N = 60) and 2.5 for HH (N = 63). Furthermore, the typical height of the DNA crossings stabilized by FIS in both constructs was consistently larger (h_{FIS} = 1.35 ± 0.15 nm, N = 60; mean ± SD) than that of DNA

Table 1. Statistical parameters of circular DNA molecules bound by FIS and H-NS (mean ± SD)

Circular DNA shape parameters

Sample	Number	$L_{(contour)}$ [nm]	ΔL (%)	l_p [nm]	R_g [nm]	ΔR_g (%)
Head-to-head						
Control	60	1280 ± 45	–	53 ± 3	145 ± 20	/
+ FIS: kb = 2.6	45	1240 ± 65	−3	35 ± 5	107 ± 15	−26
+ FIS: H-NS: kb = 2.6 : 6.8 : 1	35	1265 ± 65	−1.0	30 ± 5	105 ± 15	−27
+ H-NS: kb = 0.9	35	1110 ± 105	−13	41 ± 5	121 ± 15	−16
Head-to-tail						
Control	65	1295 ± 65	–	53 ± 3	152 ± 15	/
+ FIS: kb = 2.6	45	1260 ± 45	−2.5	27 ± 5	102 ± 10	−33
+ FIS: H-NS: kb = 2.6 : 6.8 : 1	43	1290 ± 65	−0.5	34 ± 5	105 ± 10	−31
+ H-NS: kb = 0.8	30	1180 ± 75	−9	42 ± 5	125 ± 15	−18
pBR322 control (4.4kb)						
Control	35	1370 ± 30	–	52 ± 3	162 ± 20	/
+ FIS: kb = 2.4	30	1420 ± 70	+3.5	40 ± 5	135 ± 20	−17
+ H-NS: kb = 3.7	55	1405 ± 35	+2.5	53 ± 5	155 ± 15	−4

crossings in the control samples without protein (h_{DNA} = 1.05 ± 0.15 nm, N = 60; mean ± SD) (Figure S2). This enabled us to distinguish the FIS binding position along the DNA molecules. Next, we looked at the typical loop sizes (defined as the loop contour length) formed by the binding of FIS protein. The average length of the DNA loops in FIS bound samples was 135 ± 45nm (N = 50; mean ± SD) for the HH construct and 165 ± 45nm for HT (N = 50; mean ± SD), values that in both cases were smaller than the loop size in the control sample (loop length HH control = 230 ± 70nm; N = 40; loop length HT control = 240 ± 80nm, N = 40; mean ± SD).

The nanometer resolution of the AFM enabled us to also very precisely measure the various DNA shape parameters, such as the total measured contour length, the radius of gyration, and the effective persistence length of molecules – providing an insight into the structural changes induced by the FIS binding (summarized in Table 1). The radius of gyration (R_g) describes the average globular size of the molecules (Grosberg and Khokhlov, 1994) while the persistence length (l_p) (Rubinstein and Colby, 2003), describes the stiffness of the DNA molecules. For both constructs, binding of FIS decreased the radius of gyration significantly, by roughly 30%, from the initial size of ~150 nm down to ~105 nm (Table 1). Interestingly, when we incubated FIS with a control pBR322 plasmid of a similar size (4.4kb) that was devoid of any strong FIS binding sites (Figure S3), a smaller compaction rate was observed. At similar FIS concentrations, we observed only a 17% compaction. The average number of loops, however, increased by ~3 times (i.e., similar as in the HT and HH constructs) from 0.6 (N = 118) to 1.9 (N = 85), indicating FIS was still binding the DNA molecule independent of high-affinity binding sites. The effective persistence length of the DNA molecules was also affected by the binding of FIS, decreasing from 52 ± 3 nm (N = 35, error is SD) to 40 ± 5 nm (N = 30, error is SD) as expected by the observed looping of DNA. Notably, the contour length of the DNA was not much changed by FIS binding (Table 1), in contrast for H-NS binding where we saw a clear compaction.

Next, we imaged the nucleoprotein complexes formed in the presence of both FIS and H-NS with the HT and HH constructs. In our experiments, we used a FIS monomer to DNA bp ratio of 0.0026, and H-NS monomer to DNA bp ratio of 0.0066, protein concentrations that were lower by about an order of magnitude than the maximum physiological levels in the cell (Azam et al., 1999). On both constructs, we observed regions where the DNA duplexes were either bridged into plectonemic braids (as based on the DNA contour length shortening) or were crossing each other to form loops (Figure 2), that is, the characteristic shapes induced by H-NS and FIS nucleoprotein complexes, respectively. Thus, at the used near-physiological protein concentrations, both FIS and H-NS could bind naked DNA independently, forming their characteristic nucleoprotein structures. Measurements indicated that the number of DNA crossovers on both constructs

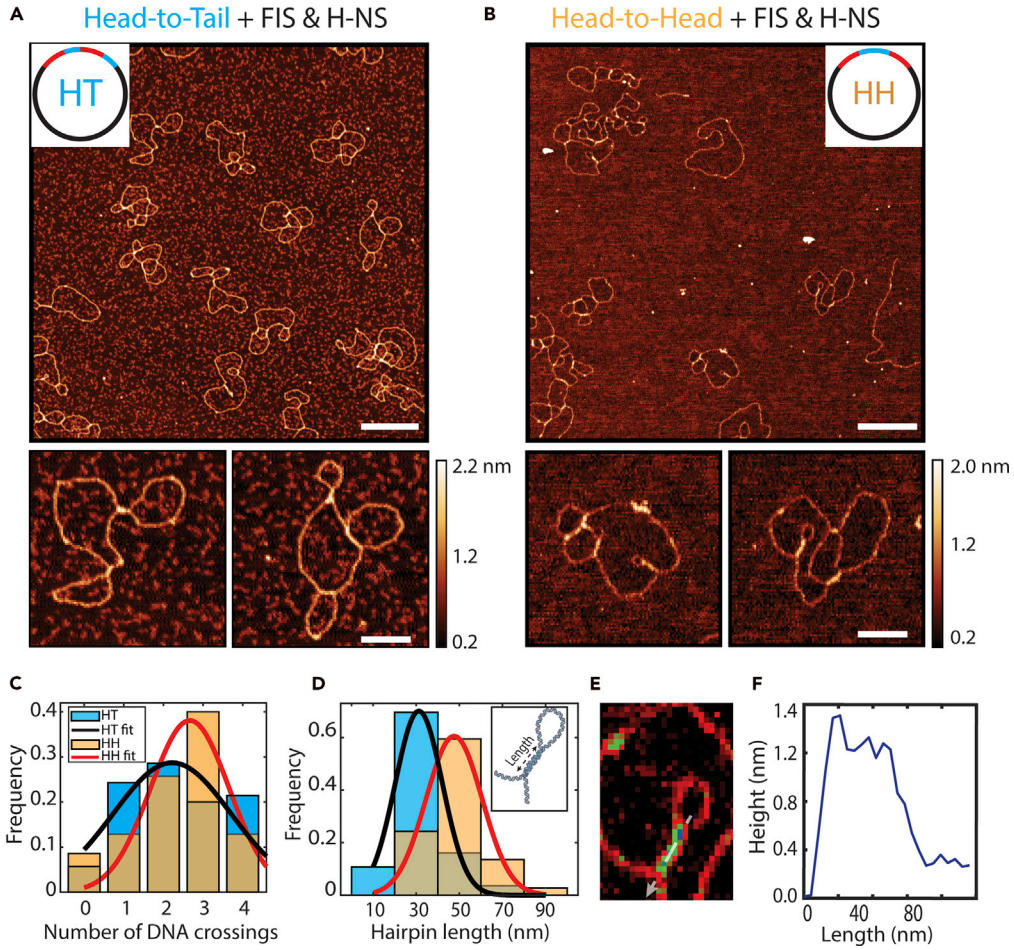

Figure 2. AFM images of FIS and H-NS nucleoprotein complexes formed on HT and HH constructs

(A) The HT construct forms looped structures indicative of FIS binding, adjoined by DNA bridges indicative of H-NS binding.

(B) The HH construct forms hairpin-like structures where the two proteins appear organized in a specific binding arrangement. Scale bars: 200nm for large scale images and 100nm for magnified images.

(C) The number of DNA crossings is similar for both HT and HH constructs. d. The length of the bridged DNA segments is larger for the HH (N = 43) than for the HT (N = 56) constructs. Solid lines denote Gaussian fits. e. Zoomed-in AFM image of the hairpin structure formed on the HH construct. f. Corresponding height cross section (indicated by dotted line on panel e).

was comparable to each other (Figure 2C) as well as to the number of crossovers obtained with FIS alone (Figures 1C and 1D). By contrast, contour length measurements showed that, on average, the bridged duplex regions formed on HH constructs were significantly more extended compared to HT (Figure 2D). On average, in HH DNA the region with bridged duplexes was 47 $\pm$ 12nm in length, (N = 43, mean $\pm$ SD), while the bridged regions observed in HT constructs were much shorter in length, 33 $\pm$ 12 nm (N = 56, mean $\pm$ SD). These latter bridged regions are shorter in contour length compared to the bridged regions formed by H-NS only, as reported earlier (Japaridze et al., 2017b).

Furthermore, on the HH construct, peculiar hairpin-like structures consisting of a "stem" of bridged DNA duplexes with a protruding loop were observed (Figures 2B and 2E), while no such structures were observed with the HT construct, suggesting that they were produced by a cooperative binding effect of FIS and H-NS to DNA with a specific (HH) arrangement of cognate binding sites.

Notably, earlier AFM studies measuring the DNA plectonemes stabilized by H-NS on both HH and HT constructs as well as on linear phage lambda DNA, reported uniform height values of ~1 nm along the H-NS

bridged regions (Japaridze et al., 2017b; Maurer et al., 2009). By contrast, height measurements of H-NS bridged duplexes in the hairpin structures formed on the HH constructs with the mixture of FIS and H-NS demonstrated non-uniform heights that varied between the stem of the bridged DNA and the base of the loop, i.e., the point where the DNA duplexes became disjointed (Figures 2E and 2F). The stem was typically ~ 1nm in height, while the height of the crossings abutting the diverging duplexes was 1.45 ± 0.2 nm (N = 60, error is SD) (Figure 2F), remarkably close to the values obtained for FIS binding (Figure S2). Given the propensity of FIS to stabilize DNA loops and high crossovers (Japaridze et al., 2017a; Maurer et al., 2006; Schneider et al., 2001; Skoko et al., 2006) and that of H-NS to form bridged DNA duplexes of uniform height, it is reasonable to assume that the peculiar DNA hairpins observed in HH constructs represent nucleoprotein complexes formed by cooperative binding of H-NS and FIS at this DNA sequence. We estimate that FIS stabilizes the base of the loop whereas H-NS bridges the DNA duplexes and forms the stem of the hairpin. We emphasize that the HT and HH constructs differ only in the spatial arrangement of the sequences with the H-NS and FIS binding sites. Therefore, it is remarkable that binding of H-NS and FIS to these two constructs can lead to the formation of such distinct structures only on one (HH) construct but not on the other (HT).

Nanopores show that nucleoprotein complexes are different in bulk

To rule out that the differences observed between the HT and HH nucleoprotein complexes represent an artifact of AFM imaging on the mica surface, we investigated the formation of these nucleoprotein complexes in solution with the use of solid-state nanopores. Apart from serving as a complementary technique to AFM in assessing the formation of nucleoprotein complexes in solution, nanopores also enabled us to gather good statistics (hundreds of DNA translocation events for each experiment). Essentially, the method involves measuring the electrophoretically driven translocation of DNA molecules across a nanometer-sized pore (15 nm diameter in our case) with an applied voltage (see transparent methods), as shown in Figure 3A. During the translocation of the molecules across the pore, the DNA temporarily disrupts the flow of ions (LiCl solution in this case) which leads to a current blockade. As schematically illustrated in Figure 3B, one can distinguish the level of folding and compaction of DNA molecules based on their current blockade levels (Kumar Sharma et al., 2019; Plesa and Dekker, 2015; Plesa et al., 2016) and see if the molecules are bound by proteins (Yang et al., 2018).

If the HH and HT nucleoprotein complexes were different in their levels of compaction, one would expect to see different blockade levels between the two constructs. As expected, both the HT and HH-DNA plasmid-only controls yielded consistent DNA events with a regular depth in the current blockades (Figures S4 and S5). After preincubation of the HH and HT DNA molecules with FIS and H-NS (see transparent methods), we observed that the HT-DNA showed deeper blockade events (Figure 3C) compared to the HH-DNA (Figure 3D) indicative of more extensive protein binding (Figure S4). Furthermore, for HH-DNA (as well as for HT), the blockade events in the presence of both FIS and H-NS were uniform and homogeneous, whereas separate addition of individual NAPs to the HH construct resulted in heterogeneous blockade levels (Figure S5). We set a threshold to select for protein bound molecules and then we quantified the percentage of events as compared to the control. Figures 3E and 3F show a relative increase in the number of deep events for the HT and HH cases in the presence of both proteins. We observed a 1.65 ± 0.06-fold increase in the number of deep events for the HT construct, but only a 1.19 ± 0.07-fold increase for the HH construct. These data are consistent with the AFM data showing that the NAPs binding of the HT construct results in an increased compaction compared to the HH construct, consistent with longer hairpins, irrespective of the used threshold (Figure S5K).

Taken together, our results indicate that spatial organization of the FIS and H-NS binding sites in the DNA is determining the 3D architecture of the nucleoprotein complexes.

DNA sequence arrangement governs the 3D nucleoprotein structure

The only difference between the nicked circular HH and HT constructs resides in the 1.4kb DNA region comprising different arrangements of the UAS and NRE sequences. We studied these 1.4kb regions on linear DNA fragments to test whether they could drive organization of different nucleoprotein assemblies, and whether the observed distinct hairpin structures could still form with the HH (UAS-NRE-NRE-UAS) as opposed to the HT (UAS-NRE-UAS-NRE) arrangement of the DNA sequence.

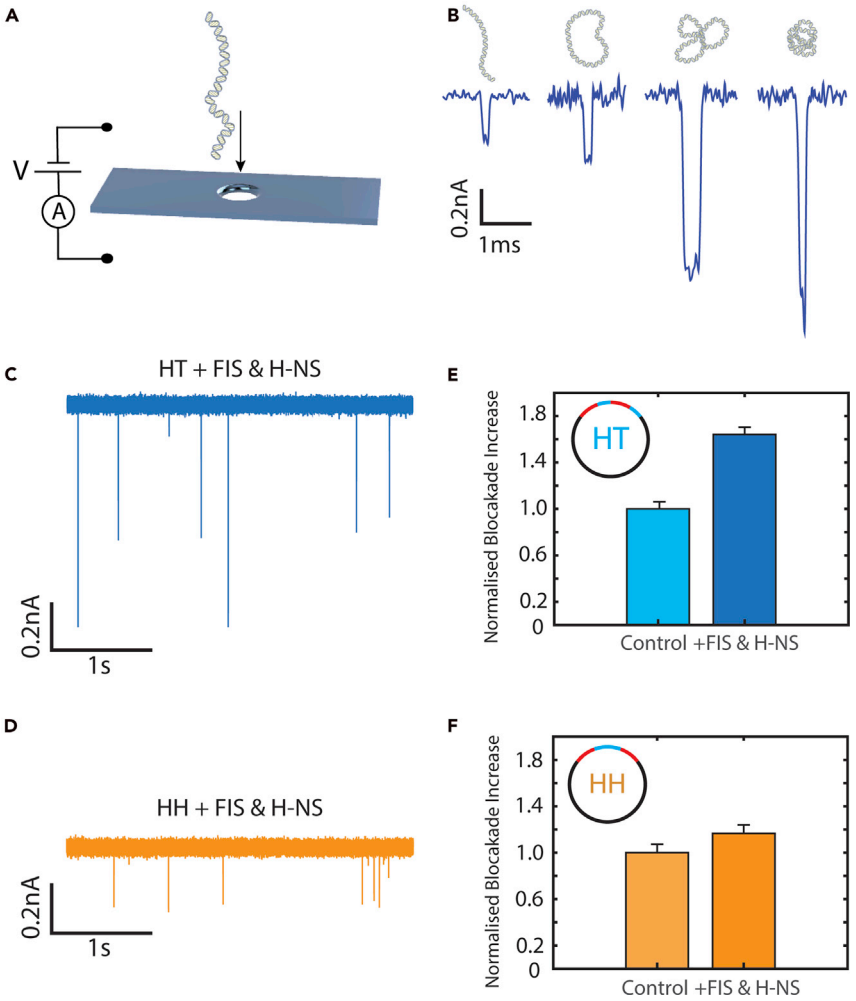

Figure 3. Nanopore experiments

(A) Schematics depicting the translocation of a DNA through a nanopore.

(B) Typical blockade events for HT DNA construct passing through a nanopore.

(C) Typical nanopore traces for the HT + FIS & H-NS samples (1ng/μl final DNA concentration).

(D) Typical nanopore traces for HH + FIS & H-NS samples (1ng/μl final DNA concentration). Upon the protein addition, the blockades become deeper, indicative of protein binding. The blockade events for the HH + FIS & H-NS samples are uniform and homogeneous, indicating that the DNA-protein complexes are similarly organized.

Normalized blockade events for the (E) HT and (F) HH constructs, showing that the deeper events occur much more frequently for the HT construct (in 38% of total events, $N_{HT+\ Protein}$ = 277 out of 737 total events), but not for the HH construct (in 18% of total events, $N_{HH+Protein}$ = 329 out of 1812 total events). Errors bars on panels (E) and (F) indicate five times the rms of the signal noise.

Hence, we incubated the 1.4 kb linear HH and HT fragments with either FIS or H-NS, or a mixture of both under conditions similar to those used for the circular substrates. We found that binding of FIS alone stabilized the looped structures (Figures 4 and S6C), but we observed clear differences between the two constructs. The HT fragment typically formed single 'lasso' type structures, while the HH fragment formed 'butterfly' structures with multiple loops (Figures 4C and S6C). The 'lasso' structure is consistent with interaction between the FIS-UAS nucleoprotein complexes formed by binding of FIS at the UAS regions located one at the middle and one at the end of the HT fragment, whereas the 'butterfly' structure is consistent with interactions between the FIS molecules binding at the UAS regions located at the extremities of the HH fragment. The average number of DNA crossings formed upon FIS binding also increased differently for the two constructs. For the HH fragment, the looping number increased by almost three times (from 0.67 (N = 104) to 1.95 crossings (N = 80)), while for the HT it increased by more than two times (from 0.55

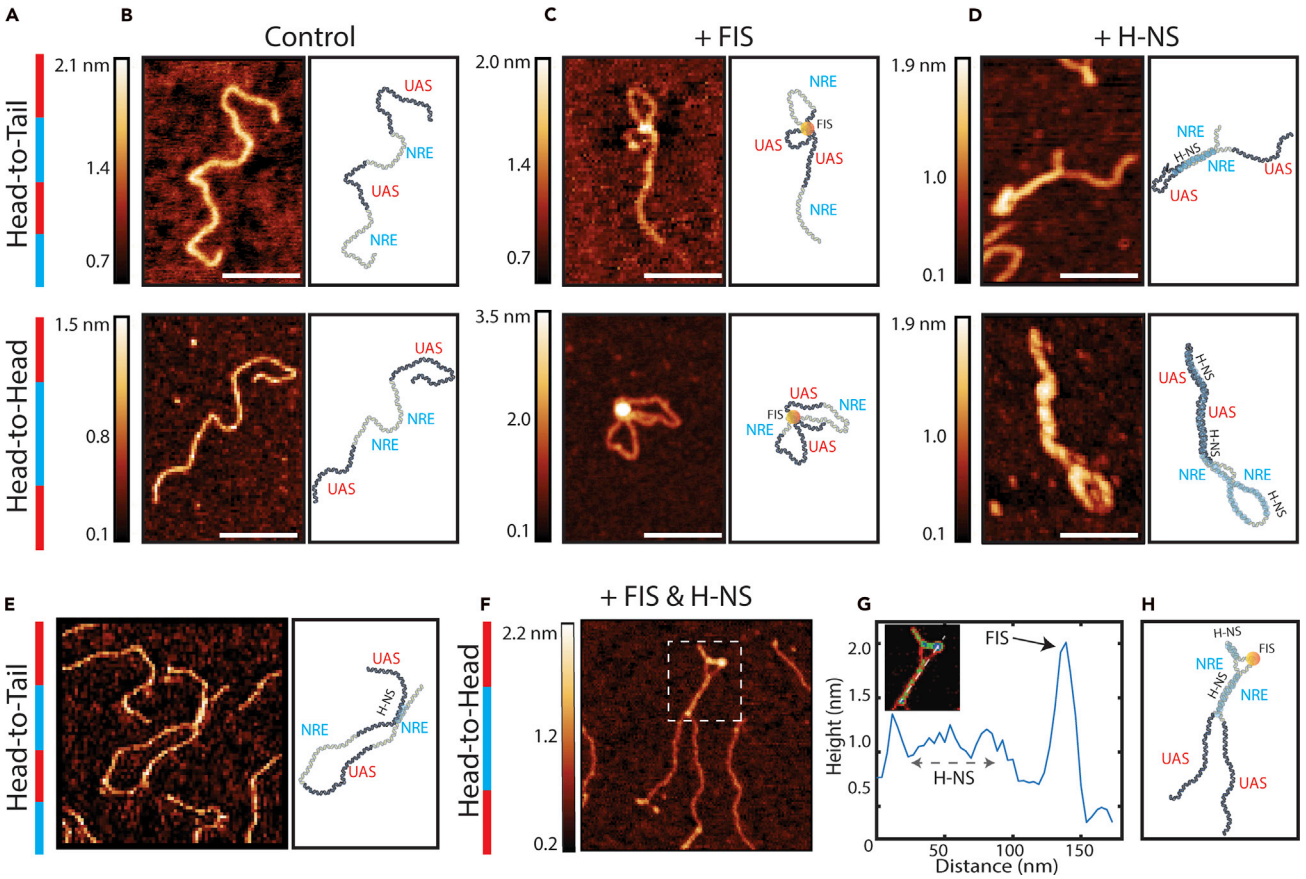

Figure 4. AFM images of nucleoprotein complexes formed on linear 1.4kb fragments

(A–H) (A) Schematic depiction of the head-to-tail (HT) and head-to-head (HH) constructs. Blue indicates the NRE and red UAS regions. b-h. AFM images with corresponding schematic depictions of the nucleoprotein organization for (B) control, (C) FIS-bound and (D) H-NS-bound linear fragments, (E) nucleoprotein complex formed by HT fragment bound by FIS & H-NS, and (F–H) nucleoprotein complex formed by HH fragment bound by FIS & H-NS.

(G) Height measurement of the nucleoprotein complex formed upon binding of FIS & H-NS to the HH fragment shown on (F). Scale bars 100nm.

(N = 111) to 1.25 crossings (N = 95)) compared to samples without the added protein. Interestingly, for both constructs, FIS formed DNA loops of a similar size ~100nm in contour length (HH L_{loop_HH} = 110 ± 35 nm (N = 43, error is SD) and HT L_{loop_HT} = 100 ± 25 nm (N = 40, error is SD), i.e., smaller in size compared to the loops formed by simple deposition of the naked DNA on surface $L_{loop\_control}$ = 150 ± 60 nm (N = 85, error is SD) (Figure S7). Similarly, as in the case of nicked circular DNA molecules, the binding of FIS compacted the structures, thereby reducing the radius of gyration and the effective persistence length (Table S1).

For the H-NS only condition, we also observed different bridged DNA duplex structures on the HT and HH linear fragments (Figure S6D). For the HT fragment, the bridged duplexes were associated with protruding ends of unequal lengths, consistent with H-NS bridging of the NRE sequences located once at the end and once in the middle of the fragment. For the HH fragment, the bridged duplexes did not demonstrate any protruding ends, consistent with a previously observed configuration (Japaridze et al., 2017b), in which the two adjacent NRE regions engaging all the four consecutive high-affinity nucleation sites are collinearly intertwined (Figure 4D). Again, the bridged regions were of different lengths, being shorter in HT arrangement, L_{bridge_HT} = 45 ± 25 nm (N = 43, error is SD) compared to HH L_{bridge_HH} = 65 ± 40 nm (N = 36, error is SD). What was surprising to see was that on both the HT and HH fragments, the looped DNA regions connecting the H-NS-bridged duplexes appeared to be also covered by H-NS (Figure S8). This demonstrated that under the same environmental conditions H-NS could both polymerize on individual DNA duplexes (Lim et al., 2012) as well as form bridges between two DNA double strands (Dame et al., 2000; Japaridze et al., 2017a, 2017b; Maurer et al., 2009; van der Valk et al., 2017).

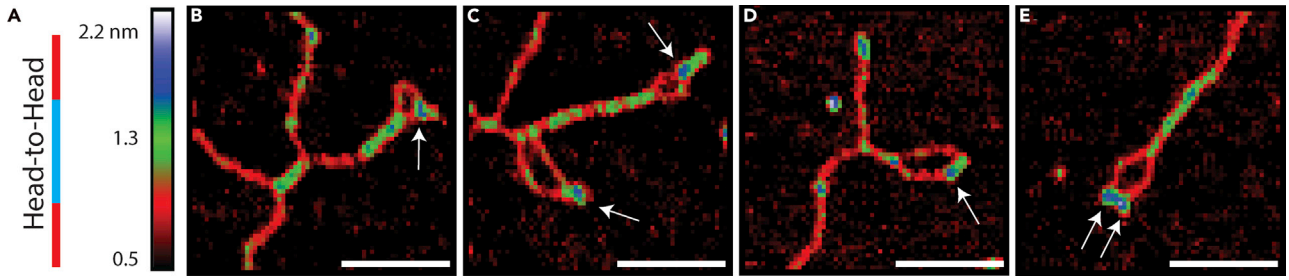

Figure 5. FIS and H-NS proteins phase separate when binding to the DNA

(A) Schematic depiction of the Head-to-Head (HH) construct. Blue indicates the NRE and red UAS regions.

(B–E) Typical magnified AFM images of HH fragments with simultaneously bound H-NS and FIS proteins. White arrows indicate the position of FIS proteins (indicated in blue). Scale bars 100nm.

When a mixture of FIS and H-NS was incubated with linear HT fragments, no regular structures were observed, as was the case with circular HT DNA (Figure 4E). Strikingly, with HH fragments however, the binding of FIS and H-NS again formed hairpin-like structures consisting of a stem of bridged DNA duplexes associated with a loop, resembling those formed with circular HH DNA (Figures 4F and 5). Measurements revealed uniform heights across the H-NS bridged regions, whereas blobs of greater heights were associated with the loops, indicative of FIS binding. Interestingly, in contrast to circular DNA, FIS was binding not at the base but rather at the apex of the loop. We infer that the differences observed between the structural organization of nucleoprotein complexes formed with HT and HH constructs are driven by distinct spatial arrangements of the UAS and NRE elements containing the FIS and H-NS binding sites (Figures 4H and 5).

DISCUSSION

While major factors involved in regulating the global architecture of the bacterial genome become progressively resolved (Japaridze et al., 2020; Lioy et al., 2018; Mäkelä and Sherratt, 2020; Wu et al., 2019a, 2019b), the smaller-scale local architectures remains largely obscure. Given the large variations in the abundance and composition of NAPs during the bacterial growth cycle (Azam et al., 1999), it is conceivable that the nucleoid undergoes reshaping (Meyer and Grainger, 2013) with corresponding changes in the local architecture depending on the metabolic state of the cell.

In this study, we set out to investigate the role of local DNA sequence organization in the assembly of higher-order nucleoprotein structures formed by simultaneous binding of two abundant bacterial NAPs, FIS and H-NS, to different spatial arrangements of their cognate DNA binding sites. We chose FIS and H-NS because of their competing functions *in vivo*. The global "genomic silencer" H-NS forms tightly interwound plectonemic structures which impede transcription (Chen and Wu, 2005; Dame et al., 2001; Dillon and Dorman, 2010; Kotlajich et al., 2015), whereas more open DNA structures, such as toroids and DNA loops stabilized by the global transcriptional activator FIS are conducive to transcription initiation (Maurer et al., 2006; Muskhelishvili et al., 1995; Skoko et al., 2006). Furthermore, both FIS and H-NS were found to be simultaneously present in transcriptionally active regions *in vivo* (Grainger et al., 2006) where they apparently compete with each other for binding by stabilizing different DNA topologies (Afflerbach et al., 1999).

To study the nucleoprotein complexes formed by the combination of FIS and H-NS, we used two nicked DNA plasmids with a spatially different HH or HT arrangement of the NAP binding sites. Binding of individual NAPs to the circular plasmids demonstrated a conspicuous difference between the architectures of the FIS and H-NS nucleoprotein complexes, fully consistent with previous microscopic observations using supercoiled DNA (Japaridze et al., 2017a; Schneider et al., 2001). Interestingly, in contrast to H-NS, we did not find any clear differences between nucleoprotein complexes formed on the two substrates with FIS alone. However, when a combination of FIS and H-NS was used, we found that various arrangements led to structurally distinct nucleoprotein complexes. In particular, binding of FIS and H-NS to the HH arrangement of sites produced specific hairpin-like structures in which the bridged duplexes stabilized by H-NS were associated with a bent DNA loop apparently stabilized by the binding of FIS, as indicated by the AFM height measurements (Figures 2 and S2). This observation is consistent with earlier studies showing that FIS can stabilize both DNA loops and crossovers (Schneider et al., 2001; Skoko et al., 2006) and with alternative DNA curvatures implicated in the competition between FIS and H-NS binding (Afflerbach et al.,

1999). When we repeated the experiments with linear DNA fragments containing just the sequences with high-affinity protein binding sites, distinct hairpin structures were observed with the HH but not the HT substrate, although in this case FIS was apparently binding at the apex rather than at the base of the loop (Figures 4 and 5). We surmise that this difference might be explained by the so-called "antenna effect," where increase in the DNA substrate length can lead to an increased probability of protein binding to specific sequences (Shimamoto et al., 2020). However, since we could not observe such regular structures with the HT arrangement of binding sites (nor with a control PBR DNA without any strong binding sites) with either the circular or linear DNA substrates, we infer that their peculiar architecture is a result of crosstalk between FIS and H-NS driven by the specific spatial organization of the binding sequences.

In nanopore experiments, we found that the HH nucleoprotein complexes formed by FIS and H-NS demonstrated regular current blockade levels in contrast to HT (Figures 3 and S5) consistent with the AFM data suggesting higher structural regularity of the HH compared to that of the HT nucleoprotein complexes.

The organization of HH nucleoprotein complexes was shown to be due to H-NS bridging of the two adjacent NRE elements that contain high-affinity H-NS binding sites and plectonemic coiling of the DNA (Japaridze et al., 2017b). This configuration leads to tightly bent small DNA loops that are bound by FIS, as observed in our experiments (Figures 2 and 4). While at the present stage we cannot distinguish the temporal pattern of H-NS and FIS binding, such tight loops might be especially attractive for further FIS binding. First, a tightly bent DNA loop would facilitate FIS binding due to the unusually short distance between the helix-turn-helix motifs of FIS and, accordingly, a strong preference for tightly bent DNA substrates with compressed minor groove (Stella et al., 2010). Second, while the NREs demonstrate a sequence periodicity of ~11 bp, H-NS-bridging of the adjacent NREs in HH construct constrains negative superhelicity, most likely due to the right-handed plectonemic coiling and stabilization of high negative twist (Japaridze et al., 2017b). This would lead to compensatory over-twisting of the protruding loop reducing the helical repeat to values < 10.5 bp, consistent with the assumed preferential value for FIS binding of ~10.2 bp (Travers and Muskhelishvili, 2013). This over-twisting would also counteract the H-NS binding within the tight loop stabilized by FIS and lead to the organization of structures observed in Figure 5, in which FIS is positioned in the looped DNA regions surrounded by H-NS bridged DNA filaments. The loop formed between the adjacent NRE elements in HH constructs is devoid of strong FIS binding sites and we observed that FIS binds at different positions in the loop, supporting the view that it is the DNA shape rather than DNA sequence that dictates FIS binding. Interestingly, in the absence of FIS, H-NS is capable of polymerizing on the tightly bent loop connecting the bridged helices (Figures 4D and S8), meaning that FIS hinders the spread of H-NS. While this process may depend on the size and topology of the DNA substrate, further studies of nucleoprotein complexes formed with successive addition of FIS and H-NS on both circular and linear substrates will help to clarify this question. The exact mechanism of this cooperation between FIS and H-NS is not yet resolved, but it is likely mediated by the DNA structure and topology. The local arrangement of FIS and H-NS proteins in the HH hairpins is non-random. This suggests that some form of DNA-driven phase separation could drive a differentiation of the bacterial chromatin architecture (Barbieri et al., 2012; Brackley and Marenduzzo, 2020). The heterogeneity in binding site arrangement could be utilized by abundant DNA architectural proteins to drive the differentiation of chromatin architecture and gene transcription as observed for H-NS filaments both *in vivo* and *in vitro* by the Landick group (Shen et al., 2020). Notably, recent studies demonstrated that the physiological B-form DNA can undergo structural changes resulting in non-canonical DNA forms under the influence of DNA supercoiling (Pyne et al., 2021), spatial confinement (Japaridze et al., 2017c), and DNA sequence (Du and Zhou, 2013; Dumat et al., 2016), indicating that the DNA structure itself is highly heterogeneous and can be favorable for protein binding based on structure rather than sequence. Our observations are in keeping with the reported capacity of FIS and H-NS to form topological barriers in the chromosome (Hardy and Cozzarelli, 2005). Looped regions stabilized by FIS that are not bound by H-NS, could potentially create patches of "open" and "closed" DNA regions differentially accessible to transcription machinery (Kane and Dorman, 2011). These coexisting structures are in line with the predominantly repressing and activating roles of H-NS and FIS on transcription, respectively. Since the distribution of the NAP binding sites in genomes of bacteria is non-random (Dillon et al., 2012; Lang et al., 2007; Ussery et al., 2001), we hypothesize that the growth-phase-dependent regulation of transcription (Blot et al., 2006) involves global alterations of chromatin accessibility. This accessibility is modulated by a crosstalk between temporally changing composition of NAPs and a non-random distribution of their cognate genomic binding sites, thus leading to spatiotemporal organization of the "open" and "closed" DNA configurations pertinent to genomic expression.

Limitations of the study

AFM imaging does not permit base-pair DNA resolution and gives only the overall morphology without knowing the exact bp positions where the proteins are bound. Furthermore, DNA in bacteria is typically supercoiled, indicating that conclusions made for linear DNA should be considered with caution when extrapolating to supercoiled DNA. The protein-DNA binding modes for H-NS and FIS as well as DNA binding strength are strongly salt dependent. High-salt experiments are required for the signal in nanopore sensing. For these nanopore experiments, the proteins were pre-bound and then transferred to the high salt condition, which in turn can lead to the dissociation of proteins from the DNA over time which places a limitation of measurement time.

To assess the relevancy of the *in vivo* observations, it would be useful to have an estimate of the natural occurrence of such HH and HT configurations in bacterial genomes. These proposals merit further independent investigations.

Resource availability

Lead contact

Information and requests for resources should be directed to and will be fulfilled by the lead contact, Aleksandre Japaridze (a.japaridze@tudelft.nl).

Materials availability

This study generated no unique materials.

Data and code availability

All relevant data are available from the lead contact upon request. Original AFM data underlying the data reported in Figures 1,2,4 and 5 in the main text are available online via Mendeley Data repository with DOI link at https://doi.org/10.17632/4xvnyx47b5.1.

METHODS

All methods can be found in the accompanying Transparentmethods supplemental file.

SUPPLEMENTALINFORMATION

Supplemental information can be found online at https://doi.org/10.1016/j.isci.2021.102408.

ACKNOWLEDGMENTS

The work was supported by the Netherlands Organisation for Scientific Research, the Netherlands (NWO/OCW), as part of the NanoFront and BaSyC programs. C.D. acknowledges support byERC Advanced GrantSynDiv (no. 669598). A.J. acknowledges support by the Swiss National Science Foundation, Switzerland (Grants P2ELP2_168554 and P300P2_177768).

AUTHOR CONTRIBUTIONS

A.J. and G.M. conceived, designed, and supervised the project. A.J. constructed DNA fragments and performed AFM measurements and analysis. W.Y. performed nanopore measurements and analysis. W.N. performed protein purification. All authors contributed to the project concept, data interpretation, and writing the manuscript.

DECLARATION OF INTERESTS

The authors declare no competing interests.

Received: November 20, 2020
Revised: March 5, 2021
Accepted: April 6, 2021
Published: May 21, 2021

REFERENCES

Afflerbach, H., Schröder, O., and Wagner, R. (1999). Conformational changes of the upstream DNA mediated by H-NS and FIS regulate E. coli rrnB P1 promoter activity. J. Mol. Biol. *286*, 339–353.

Azam, T.A., Iwata, A., Nishimura, A., Ueda, S., and Ishihama, A. (1999). Growth phase-dependent variation in protein composition of the Escherichia coli nucleoid. J. Bacteriol. *181*, 6361–6370.

Badaut, C., Williams, R., Arluison, V., Bouffartigues, E., Robert, B., Buc, H., and Rimsky, S. (2002). The degree of oligomerization of the H-NS nucleoid structuring protein is related to specific binding to DNA. J. Biol. Chem. *277*, 41657–41666.

Ball, C.A., and Johnson, R.C. (1991). Efficient excision of phage λ from the Escherichia coli chromosome requires the FIS protein. J. Bacteriol. *173*, 4027–4031.

Ball, C.A., Osuna, R., Ferguson, K.C., and Johnson, R.C. (1992). Dramatic changes in FIS levels upon nutrient upshift in Escherichia coli. J. Bacteriol. *174*, 8043–8056.

Barbieri, M., Chotalia, M., Fraser, J., Lavitas, L.M., Dostie, J., Pombo, A., and Nicodemi, M. (2012). Complexity of chromatin folding is captured by the strings and binders switch model. Proc. Natl. Acad. Sci. U S A. *109*, 16173–16178.

Berger, M., Gerganova, V., Berger, P., Rapiteanu, R., Lisicovas, V., and Dobrindt, U. (2016). Genes on a wire: the nucleoid-associated protein HU insulates transcription units in Escherichia coli. Sci. Rep. *6*, 31512.

Blot, N., Mavathur, R., Geertz, M., Travers, A., and Muskhelishvili, G. (2006). Homeostatic regulation of supercoiling sensitivity coordinates transcription of the bacterial genome. EMBO Rep. *7*, 710–715.

Bokal, A.J., Ross, W., and Gourse, R.L. (1995). The transcriptional activator protein FIS: DNA interactions and cooperative interactions with RNA polymerase at the Escherichia coli rrnB P1 promoter. J. Mol. Biol. *245*, 197–207.

Bouffartigues, E., Buckle, M., Badaut, C., Travers, A., and Rimsky, S. (2007). H-NS cooperative binding to high-affinity sites in a regulatory element results in transcriptional silencing. Nat. Struct. Mol. Biol. *14*, 441–448.

Brackley, C.A., and Marenduzzo, D. (2020). Bridging-induced microphase separation: photobleaching experiments, chromatin domains and the need for active reactions. Brief. Funct. Genomics *19*, 111–118.

Brunetti, R., Prosseda, G., Beghetto, E., Colonna, B., and Micheli, G. (2001). The looped domain organization of the nucleoid in histone-like protein defective Escherichia coli strains. Biochimie *83*, 873–882.

Chen, C.C., and Wu, H.Y. (2005). LeuO protein delimits the transcriptionally active and repressive domains on the bacterial chromosome. J. Biol. Chem. *280*, 15111–15121.

Dages, S., Zhi, X., and Leng, F. (2020). FIS protein forms DNA topological barriers to confine transcription-coupled DNA supercoiling in Escherichia coli. FEBS Lett. *594*, 791–798.

Dame, R.T., Wyman, C., and Goosen, N. (2000). H-NS mediated compaction of DNA visualised by atomic force microscopy. Nucleic Acids Res. *28*, 3504–3510.

Dame, R.T., Wyman, C., Wurm, R., Wagner, R., and Goosen, N. (2001). Structural basis for H-NS-mediated trapping of RNA polymerase in the open initiation complex at the rrnB P1. J. Biol. Chem. *277*, 2146–2150.

Dame, R.T., Rashid, F.Z.M., and Grainger, D.C. (2020). Chromosome organization in bacteria: mechanistic insights into genome structure and function. Nat. Rev. Genet. *21*, 227–242.

Dillon, S.C., and Dorman, C.J. (2010). Bacterial nucleoid-associated proteins, nucleoid structure and gene expression. Nat. Rev. Microbiol. *8*, 185–195.

Dillon, S.C., Espinosa, E., Hokamp, K., Ussery, D.W., Casadesús, J., and Dorman, C.J. (2012). LeuO is a global regulator of gene expression in Salmonella enterica serovar Typhimurium. Mol. Microbiol. *85*, 1072–1089.

Dorman, C.J. (2007). H-NS, the genome sentinel. Nat. Rev. Microbiol. *5*, 157–161.

Driessen, R.P.C., and Dame, R.T. (2011). Nucleoid-associated proteins in Crenarchaea. Biochem. Soc. Trans. *39*, 116–121.

Du, Y., and Zhou, X. (2013). Targeting non-B-form DNA in living cells. Chem. Rec. *13*, 371–384.

Dumat, B., Larsen, A.F., and Wilhelmsson, L.M. (2016). Studying Z-DNA and B-to Z-DNA transitions using a cytosine analogue FRET-pair. Nucleic Acids Res. *44*, 101.

Fisher, J.K., Bourniquel, A., Witz, G., Weiner, B., Prentiss, M., and Kleckner, N. (2013). Four-dimensional imaging of E. coli nucleoid organization and dynamics in living cells. Cell *153*, 882–895.

Gordon, B.R.G., Li, Y., Cote, A., Weirauch, M.T., Ding, P., Hughes, T.R., Navarre, W.W., Xia, B., and Liu, J. (2011). Structural basis for recognition of AT-rich DNA by unrelated xenogeneic silencing proteins. Proc. Natl. Acad. Sci. U S A. *108*, 10690–10695.

Gowrishankar, J. (1985). Identification of osmoresponsive genes in Escherichia coli: evidence for participation of potassium and proline transport systems in osmoregulation. J. Bacteriol. *164*, 434–445.

Grainger, D.C., Hurd, D., Goldberg, M.D., and Busby, S.J.W. (2006). Association of nucleoid proteins with coding and non-coding segments of the Escherichia coli genome. Nucleic Acids Res. *34*, 4642–4652.

Grosberg, A., and Khokhlov, A. (1994). Statistical Physics of Macromolecules SE - AIP Series in Polymers and Complex Materials (AIP Press).

Hadizadeh Yazdi, N., Guet, C.C., Johnson, R.C., and Marko, J.F. (2012). Variation of the folding and dynamics of the Escherichia coli chromosome with growth conditions. Mol. Microbiol. *86*, 1318–1333.

Hardy, C.D., and Cozzarelli, N.R. (2005). A genetic selection for supercoiling mutants of *Escherichia coli* reveals proteins implicated in chromosome structure. Mol. Microbiol. *57*, 1636–1652.

Hatfield, G.W., and Benham, C.J. (2002). DNA topology-mediated control of global gene expression in Escherichia coli. Annu. Rev. Genet. *36*, 175–203.

Hirvonen, C.A., Ross, W., Wozniak, C.E., Marasco, E., Anthony, J.R., Aiyar, S.E., Newburn, V.H., and Gourse, R.L. (2001). Contributions of UP elements and the transcription factor FIS to expression from the seven rrn P1 promoters in Escherichia coli downloaded from. J. Bacteriol. *183*, 6305–6314.

Japaridze, A., Muskhelishvili, G., Benedetti, F., Gavriilidou, A.F.M.A.F.M., Zenobi, R., De Los Rios, P., Longo, G., and Dietler, G. (2017a). Hyperplectonemes: a higher order compact and dynamic DNA self-organization. Nano Lett. *17*, 1938–1948.

Japaridze, A., Renevey, S., Sobetzko, P., Stoliar, L., Nasser, W., Dietler, G., and Muskhelishvili, G. (2017b). Spatial organization of DNA sequences directs the assembly of bacterial chromatin by a nucleoid-associated protein. J. Biol. Chem. *292*, 7607–7618.

Japaridze, A., Orlandini, E., Smith, K.B.K.B., Gmür, L., Valle, F., Micheletti, C., and Dietler, G. (2017c). Spatial confinement induces hairpins in nicked circular DNA. Nucleic Acids Res. *45*, 4905–4914.

Japaridze, A., Gogou, C., Kerssemakers, J.W.J., Nguyen, H.M., and Dekker, C. (2020). Direct observation of independently moving replisomes in Escherichia coli. Nat. Commun. *11*, 733956.

Kahramanoglou, C., Seshasayee, A.S.N., Prieto, A.I., Ibberson, D., Schmidt, S., Zimmermann, J., Benes, V., Fraser, G.M., and Luscombe, N.M. (2011). Direct and indirect effects of H-NS and Fis on global gene expression control in Escherichia coli. Nucleic Acids Res. *39*, 2073–2091.

Kane, K.A., and Dorman, C.J. (2011). Rational design of an artificial genetic switch: Co-option of the H-NS-repressed proU Operon by the VirB virulence master regulator. J. Bacteriol. *193*, 5950–5960.

Kotlajich, M.V., Hron, D.R., Boudreau, B.A., Sun, Z., Lyubchenko, Y.L., and Landick, R. (2015). Bridged filaments of histone-like nucleoid structuring protein pause RNA polymerase and aid termination in bacteria. Elife *4*, e04970.

Kumar Sharma, R., Agrawal, I., Dai, L., Doyle, P.S., and Garaj, S. (2019). Complex DNA knots detected with a nanopore sensor. Nat. Commun. *10*, 1–9.

Lamond, A.I., and Travers, A.A. (1983). Requirement for an upstream element for optimal transcription of a bacterial tRNA gene. Nature *305*, 248–250.

Lang, B., Blot, N., Bouffartigues, E., Buckle, M., Geertz, M., Gualerzi, C.O., Mavathur, R.,

Muskhelishvili, G., Pon, C.L., Rimsky, S., et al. (2007). High-affinity DNA binding sites for H-NS provide a molecular basis for selective silencing within proteobacterial genomes. Nucleic Acids Res. *35*, 6330–6337.

Lautier, T., and Nasser, W. (2007). The DNA nucleoid-associated protein Fis co-ordinates the expression of the main virulence genes in the phytopathogenic bacterium Erwinia chrysanthemi. Mol. Microbiol. *66*, 1474–1490.

Lazarus, L.R., and Travers, A.A. (1993). The Escherichia coli FIS protein is not required for the activation of tyrT transcription on entry into exponential growth. EMBO J. *12*, 2483.

Lim, C.J., Lee, S.Y., Kenney, L.J., and Yan, J. (2012). Nucleoprotein filament formation is the structural basis for bacterial protein H-NS gene silencing. Sci. Rep. *2*, 1–6.

Lioy, V.S., Cournac, A., Marbouty, M., Duigou, S., Mozziconacci, J., Espéli, O., Boccard, F., and Koszul, R. (2018). Multiscale structuring of the E. coli chromosome by nucleoid-associated and Condensin proteins. Cell *172*, 771–783.e18.

Liu, Y., Chen, H., Kenney, L.J., and Yan, J. (2010). A divalent switch drives H-NS/DNA-binding conformations between stiffening and bridging modes. Genes Dev. *24*, 339–344.

Lucchini, S., Rowley, G., Goldberg, M.D., Hurd, D., Harrison, M., and Hinton, J.C.D.D. (2006). H-NS mediates the silencing of laterally acquired genes in bacteria. Plos Pathog. *2*, 0746–0752.

Luijsterburg, M.S., Noom, M.C., Wuite, G.J.L., and Dame, R.T. (2006). The architectural role of nucleoid-associated proteins in the organization of bacterial chromatin: a molecular perspective. J. Struct. Biol. *156*, 262–272.

Mäkelä, J., and Sherratt, D.J. (2020). Organization of the Escherichia coli chromosome by a MukBEF axial core. Mol. Cell *78*, 250–260.e5.

Maurer, S., Fritz, J., Muskhelishvili, G., and Travers, A. (2006). RNA polymerase and an activator form discrete subcomplexes in a transcription initiation complex. EMBO J. *25*, 3784–3790.

Maurer, S., Fritz, J., and Muskhelishvili, G. (2009). A systematic in vitro study of nucleoprotein complexes formed by bacterial nucleoid-associated proteins revealing Novel types of DNA organization. J. Mol. Biol. *387*, 1261–1276.

Mertens, G., Klippel, A., Fuss, H., Blöcker, H., Frank, R., and Kahmann, R. (1988). Site-specific recombination in bacteriophage Mu: characterization of binding sites for the DNA invertase Gin. EMBO J. *7*, 1219–1227.

Meyer, A.S., and Grainger, D.C. (2013). The Escherichia coli nucleoid in stationary phase. Advances in Applied Microbiology (Academic Press Inc.), pp. 69–86.

Muskhelishvili, G., and Travers, A. (2003). Transcription factor as a topological homeostat. Front. Biosci. *8*, 279–285.

Muskhelishvili, G., Travers, A.A., Heumann, H., and Kahmann, R. (1995). FIS and RNA polymerase holoenzyme form a specific nucleoprotein complex at a stable RNA promoter. EMBO J. *14*, 1446–1452.

Nasser, W., and Reverchon, S. (2002). H-NS-dependent activation of pectate lyases synthesis in the phytopathogenic bacterium *Erwinia chrysanthemi* is mediated by the PecT repressor. Mol. Microbiol. *43*, 733–748.

Navarre, W.W., Porwollik, S., Wang, Y., McClelland, M., Rosen, H., Libby, S.J., and Fang, F.C. (2006). Selective silencing of foreign DNA with low GC content by the H-NS protein in Salmonella. Science *313*, 236–238.

Ninnemann, O., Koch, C., and Kahmann, R. (1992). The E.coli fis promoter is subject to stringent control and autoregulation. EMBO J. *11*, 1075–1083.

Plesa, C., and Dekker, C. (2015). Data analysis methods for solid-state nanopores. Nanotechnology *26*, 084003.

Plesa, C., Verschueren, D., Pud, S., Van Der Torre, J., Ruitenberg, J.W., Witteveen, M.J., Jonsson, M.P., Grosberg, A.Y., Rabin, Y., and Dekker, C. (2016). Direct observation of DNA knots using a solid-state nanopore. Nat. Nanotechnol. *11*, 1093–1097.

Pyne, A.L., Noy, A., S Main, K.H., Velasco-Berrelleza, V., Piperakis, M.M., Mitchenall, L.A., Cugliandolo, F.M., Beton, J.G., M Stevenson, C.E., Hoogenboom, B.W., et al. (2021). Base-pair resolution analysis of the effect of supercoiling on DNA flexibility and major groove recognition by triplex-forming oligonucleotides. Nat. Commun. *121*, 1–12.

Rubinstein, M., and Colby, R.H. (2003). Polymers Physics (Oxford University Press).

Schneider, R., Lurz, R., Lüder, G., Tolksdorf, C., Travers, A., and Muskhelishvili, G. (2001). An architectural role of the Escherichia coli chromatin protein FIS in organising DNA. Nucleic Acids Res. *29*, 5107–5114.

Schröder, O., and Wagner, R. (2000). The bacterial DNA-binding protein H-NS represses ribosomal RNA transcription by trapping RNA polymerase in the initiation complex. J. Mol. Biol. *298*, 737–748.

Shen, B.A., Hustmyer, C.M., Roston, D., Wolfe, M.B., Jessen, E.D., and Landick, R. (2020). Hybrid analysis reveals how DNA sequence governs genomic location and DNA contacts of bacterial chromatin H-NS filaments. BioRxiv. https://doi.org/10.1101/2020.06.11.146589.

Shimamoto, N., Toda, M., Nara, S., Komatsuzaki, T., Kamagata, K., Kinebuchi, T., and Tomizawa, J. (2020). Dependence of DNA length on binding affinity between TrpR and trpO of DNA. Sci. Rep. *10*, 15624.

Shin, M., Lagda, A.C., Lee, J.W., Bhat, A., Rhee, J.H., Kim, J.-S., Takeyasu, K., and Choy, H.E. (2012). Gene silencing by H-NS from distal DNA site. Mol. Microbiol. *86*, 707–719.

Skoko, D., Yoo, D., Bai, H., Schnurr, B., Yan, J., McLeod, S.M., Marko, J.F., and Johnson, R.C. (2006). Mechanism of chromosome compaction and looping by the Escherichia coli nucleoid protein fis. J. Mol. Biol. *364*, 777–798.

Sobetzko, P., Travers, A., and Muskhelishvili, G. (2012). Gene order and chromosome dynamics coordinate spatiotemporal gene expression during the bacterial growth cycle. Proc. Natl. Acad. Sci. U S A. *109*, E42–E50.

Sonnenschein, N., Geertz, M., Muskhelishvili, G., and Hütt, M.T. (2011). Analog regulation of metabolic demand. BMC Syst. Biol. *5*, 40.

Spurio, R., Dürrenberger, M., Falconi, M., La Teana, A., Pon, C.L., and Gualerzi, C.O. (1992). Lethal overproduction of the Escherichia coli nucleoid protein H-NS: ultramicroscopic and molecular autopsy. Mol. Gen. Genet. MGG *231*, 201–211.

Stella, S., Cascio, D., and Johnson, R.C. (2010). The shape of the DNA minor groove directs binding by the DNA-bending protein Fis. Genes Dev. *24*, 814–826.

Travers, A., and Muskhelishvili, G. (2005). Bacterial chromatin. Curr.Opin.Genet. Dev. *15*, 507–514.

Travers, A., and Muskhelishvili, G. (2020). Chromosomal organization and regulation of genetic function in Escherichia coli integrates the DNA analog and digital information. EcoSal Plus *9*, 1, https://doi.org/10.1128/ecosalplus.ESP-0016-2019.

Travers, A.A., and Muskhelishvili, G. (2013). DNA thermodynamics shape chromosome organization and topology. Biochem. Soc. Trans. *41*, 548–553.

Travers, A., Schneider, R., and Muskhelishvili, G. (2001). DNA supercoiling and transcription in Escherichia coli: the FIS connection. Biochimie *83*, 213–217.

Ussery, D., Larsen, T.S., Wilkes, K.T., Friis, C., Worning, P., Krogh, A., and Brunak, S. (2001). Genome organisation and chromatin structure in Escherichia coli. Biochimie *83*, 201–212.

van der Valk, R.A., Vreede, J., Qin, L., Moolenaar, G.F., Hofmann, A., Goosen, N., and Dame, R.T. (2017). Mechanism of environmentally driven conformational changes that modulate H-NS DNA-Bridging activity. Elife *6*, e27369.

Wu, F., Swain, P., Kuijpers, L., Zheng, X., Felter, K., Guurink, M., Solari, J., Jun, S., Shimizu, T.S., Chaudhuri, D., et al. (2019a). Cell boundary confinement sets the size and position of the E. coli chromosome. Curr.Biol. *29*, 2131–2144.e4.

Wu, F., Japaridze, A., Zheng, X., Wiktor, J., Kerssemakers, J.W.J., and Dekker, C. (2019b). Direct imaging of the circular chromosome in a live bacterium. Nat. Commun. *10*, 1–9.

Yang, W., Restrepo-Pérez, L., Bengtson, M., Heerema, S.J., Birnie, A., Van Der Torre, J., and Dekker, C. (2018). Detection of CRISPR-dCas9 on DNA with solid-state nanopores. Nano Lett. *18*, 6469–6474.

iScience, Volume *24*

Supplemental information

DNA sequence-directed cooperation between nucleoid-associated proteins

Aleksandre Japaridze, Wayne Yang, Cees Dekker, William Nasser, and Georgi Muskhelishvili

This SI includes:

Supplementary Figure 1-8

Supplementary Table 1

Transparent Methods

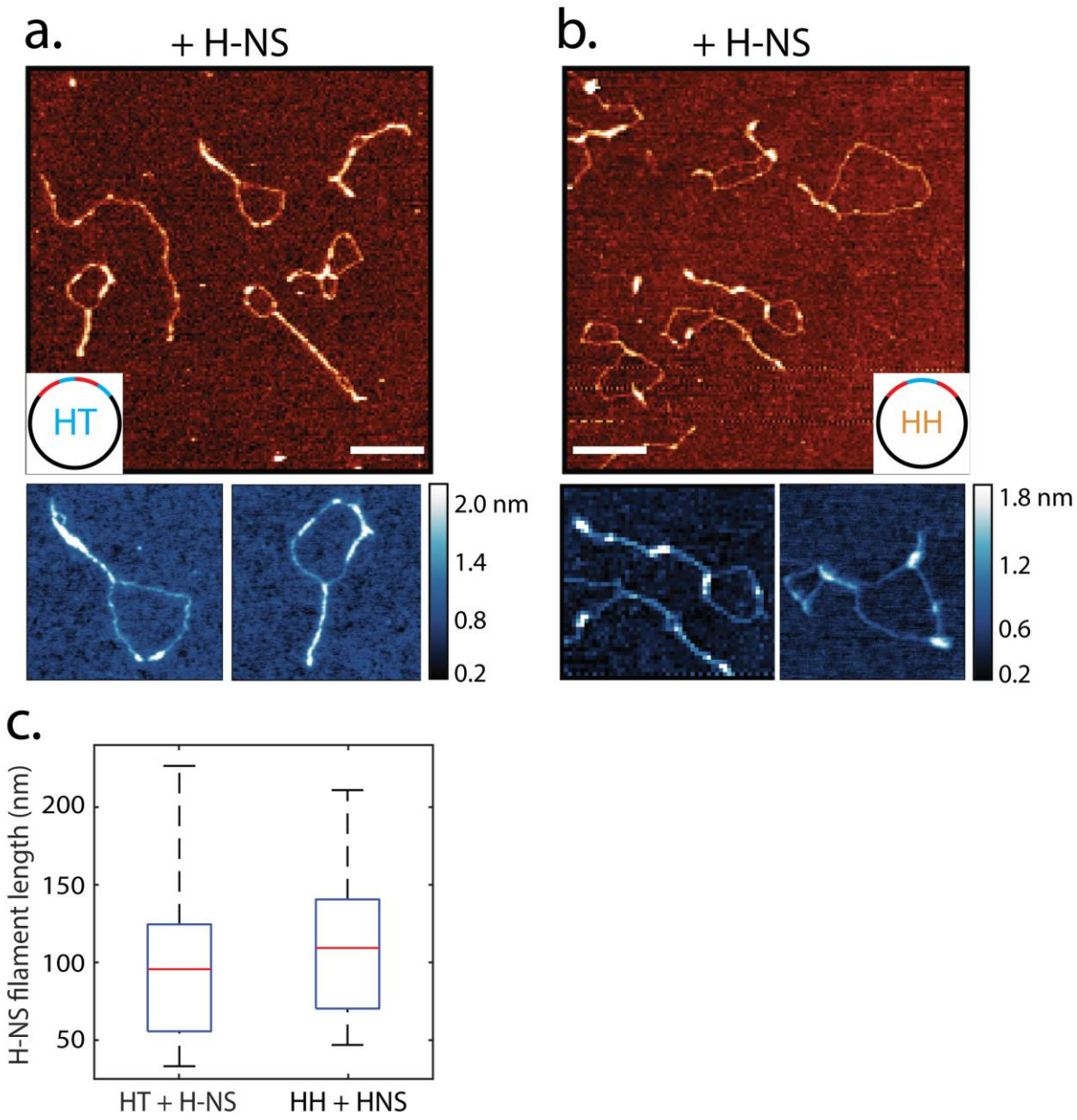

Figure S1. AFM images of **a.** HT and **b**. HH circular constructs bound by H-NS protein. The binding of H-NS stabilizes DNA bridges. Scale bars 200nm. **c.** Boxplots of filament length formed upon H-NS binding on HT and HH constructs (each sample N=35). H-NS forms longer filaments with HT construct compared to HH. The central mark indicates the median while the bottom and top edges of the box indicate the 25th and 75th percentiles, respectively. Related to Figure 1.

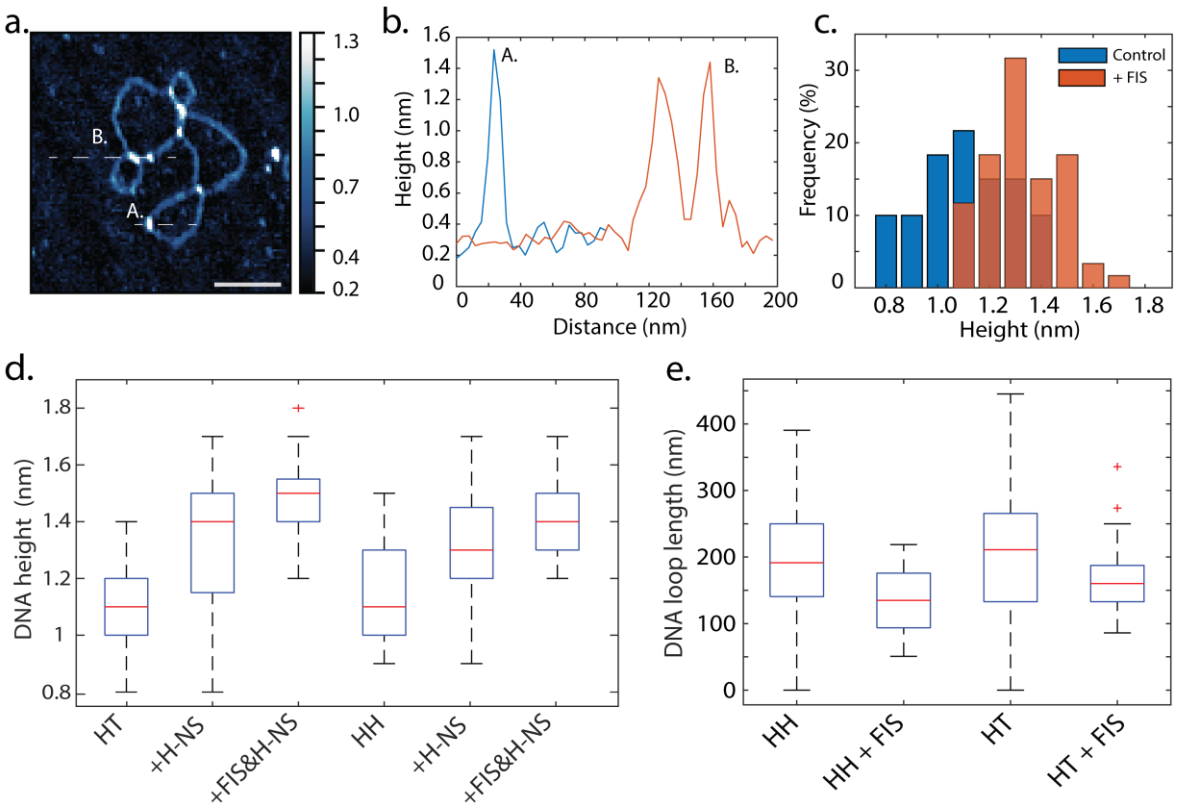

Figure S2. a. AFM images of HT plasmid bound by FIS protein. Scale bar 100nm. **b**. Height measurement along the FIS proteins bound to the DNA marked as two dotted lines in panel a. **c.** Height distributions of DNA crossings in HT control (blue) and HT + FIS (red) samples. N=60 for both samples. **d.** Boxplots of height distributions of DNA crossings in control HT and HH constructs, and protein bound ones (each sample N=60). The binding of FIS proteins significantly increases the DNA height. The central mark indicates the median while the bottom and top edges of the box indicate the 25th and 75th percentiles, respectively. **e.** Boxplots of DNA loop sizes in control (N=40 each) and FIS bound (N=50 each) HT and HH constructs. Binding of FIS forms smaller loops compared to loops formed by random DNA deposition. Related to Figure 1 & 2.

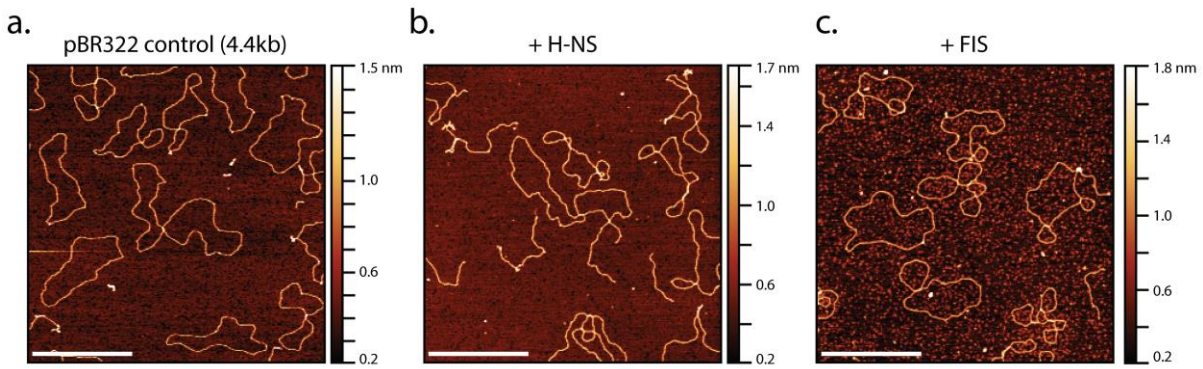

Figure S3. AFM images **a.** Control pBR322 plasmid; **b.** H-NS bound pBR322 and **c.** FIS bound pBR322. Control plasmid shows no or single DA crossings, H-NS bound plasmid shows bridged DNA regions, while FIS bound plasmid displays multiple DNA crossings. Scale bar 500nm. Related to Figure 1.

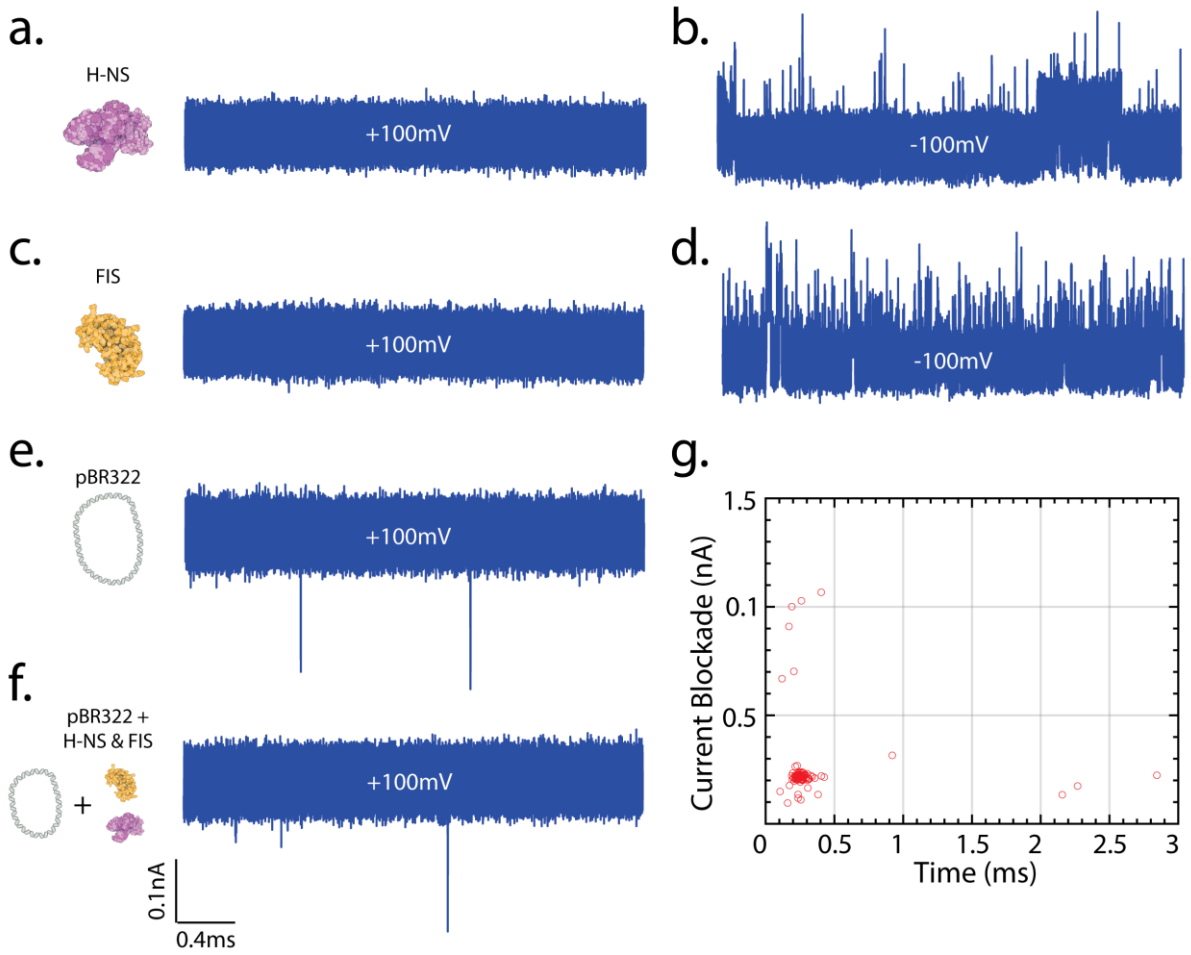

Figure S4. Typical current traces: Protein and pBR322 control experiments in a nanopore. Experiments were performed in a 20 nm nanopore in 1M LiCl. **a.** & **b**. Sample current trace with nanopore with H-NS. H-NS was introduced into the cis side of the nanopore. Only when a negative voltage (opposite to the applied voltage for DNA) can protein translocations be detected**. c.** & **d.** Sample current trace with nanopore with FIS. Similar to H-NS, the proteins are seen only when a negative voltage was applied. **e.** Sample current trace with nicked pBR322 (1ng/µl) plasmid (N=173). **f.** Sample current trace with pBR322 incubated with H-NS and Fis (1ng/µl). **g**. Collected scatter plot from pBR322 + H-NS + FIS sample (N=107). Unlike HT plasmid, we do not observe an increased current blockade upon binding of the proteins (only 6 deep blockade events out of 107). Related to Figure 3.

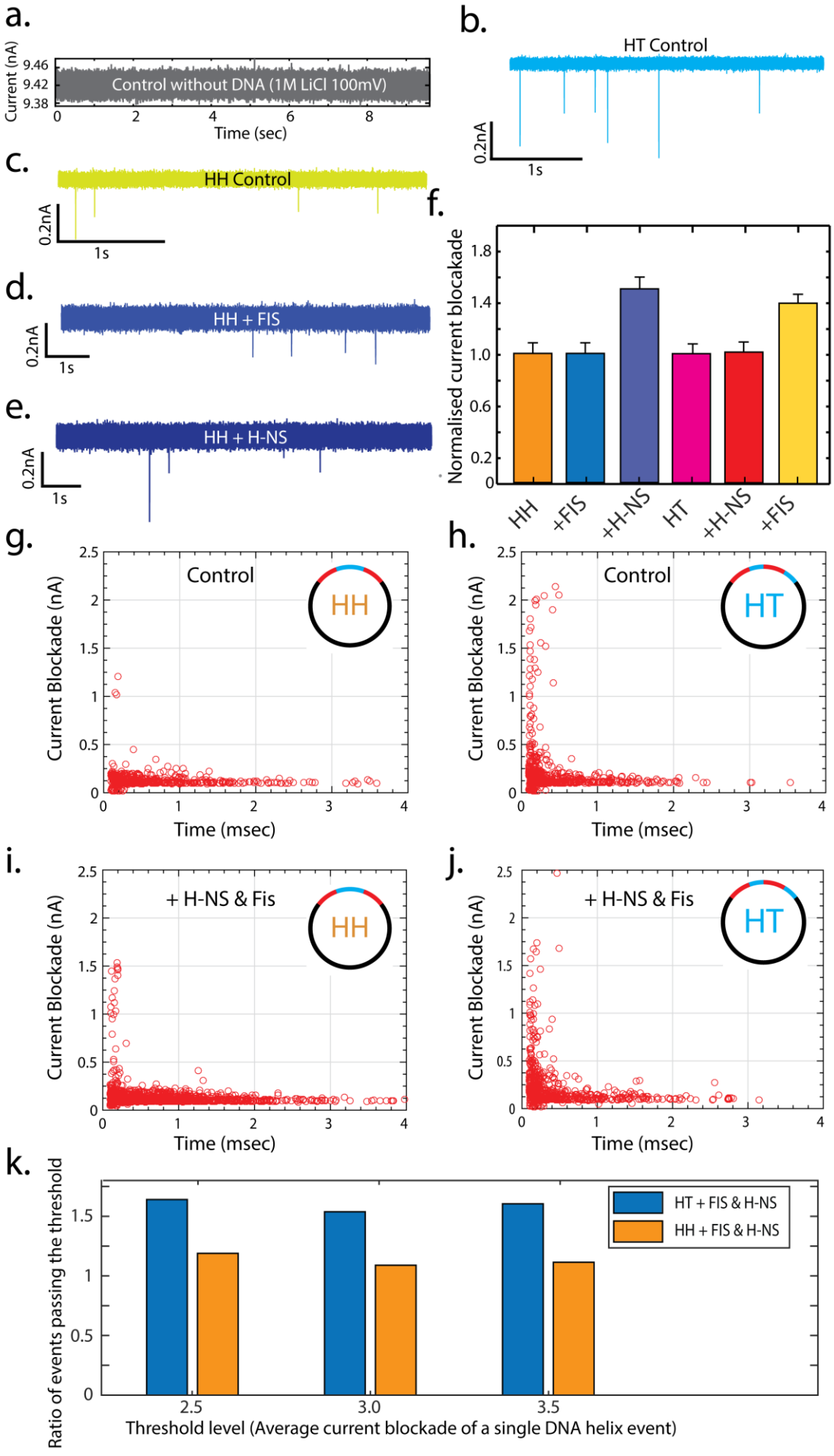
a.
Current (nA)
9.46
9.42
9.38
Control without DNA (1M LiCl 100mV)
0
2
4
6
8
Time (sec)
b.
HT Control
0.2nA
1s
c.
HH Control
0.2nA
1s
d.
HH + FIS
0.2nA
1s
e.
HH + H-NS
0.2nA
1s
f.
Normalised current blocakade
1.8
1.4
1.0
0.6
0.2
0
HH
+FIS
+H-NS
HT
+H-NS
+FIS
g.
Control
HH
Current Blockade (nA)
Time (msec)
h.
Control
HT
Current Blockade (nA)
Time (msec)
i.
+ H-NS & Fis
HH
Current Blockade (nA)
Time (msec)
j.
+ H-NS & Fis
HT
Current Blockade (nA)
Time (msec)
k.
HT + FIS & H-NS
HH + FIS & H-NS
Ratio of events passing the threshold
2.5
3.0
3.5
Threshold level (Average current blockade of a single DNA helix event)

Figure S5. Typical current traces of **a.** control sample without any DNA, not showing any translocations. **b.** HT control, **c.** HH control, **d.** HH construct bound with FIS, **e.** HH construct bound by H-NS, showing that with individual proteins we get deep and heterogeneous blockades, indicating various levels of nucleoprotein compaction. **f.** Normalized current blockade events for HH & HT construct in the presence of single proteins. HH control (N=491), HH + Fis (N=771), HH + H-NS (N=514), HT control (N=434), HT + H-NS (N=905), HT + Fis (N=968). **g.** Current blockade vs. blockade time scatter plots for control (N=491) and **h.** H-NS & FIS bound HH samples (N=1812). **i.** Current blockade vs. blockade duration scatter plots for control (N=707) and **j.** H-NS & FIS bound HT samples (N=737). **k**. The ratio of events passing the current threshold for HT and HH construct in the presence of FIS and H-NS proteins (threshold is in units of average current blockade of a single DNA). Related to Figure 3.

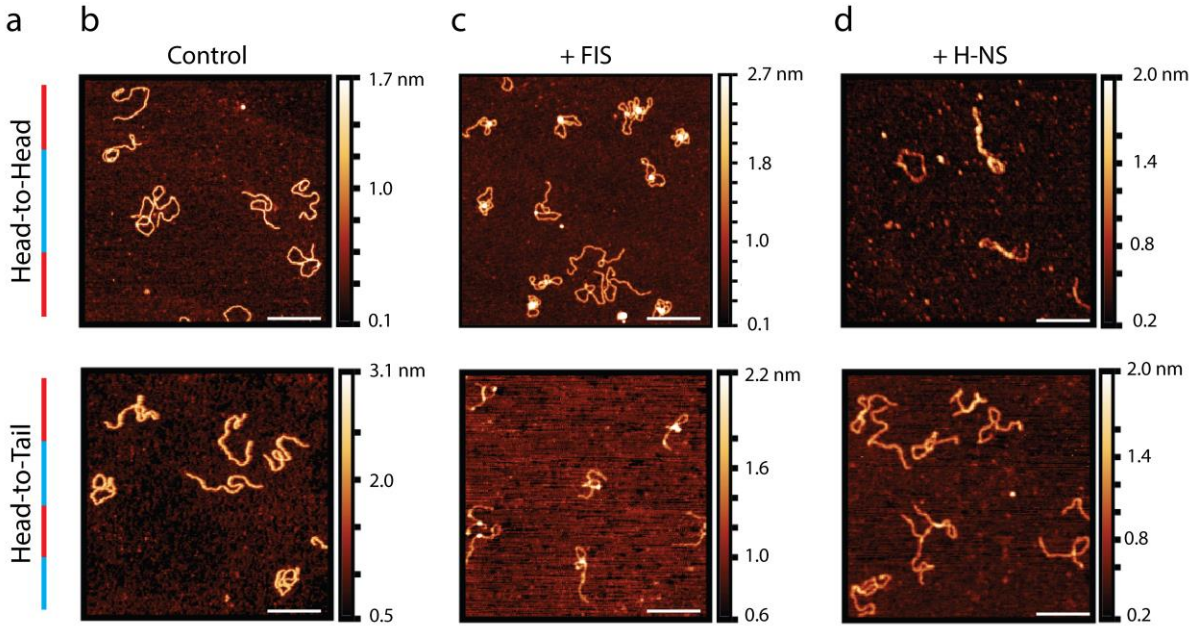

Figure S6. a. Schematic of the sequence organisation of the 1.4kb HH and HT linear fragments. Large scale AFM images of **b.** control; **c.** FIS-bound and **d.** H-NS-bound linear fragments. Scale bar 200nm. Related to Figure 4.

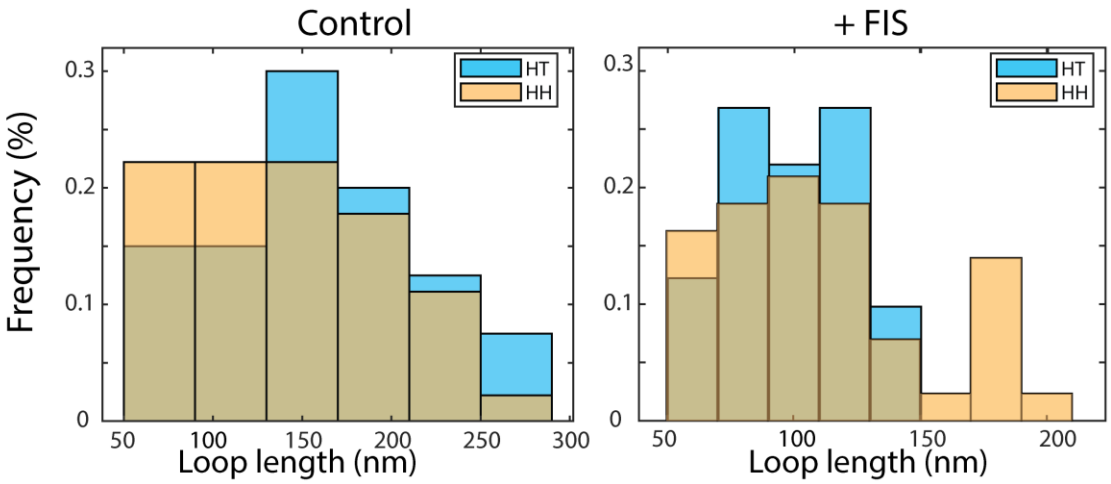

Figure S7. Loop sizes formed by the binding of FIS on linear HT (blue bars) and HH (yellow bars) fragments. Related to Figure 4.

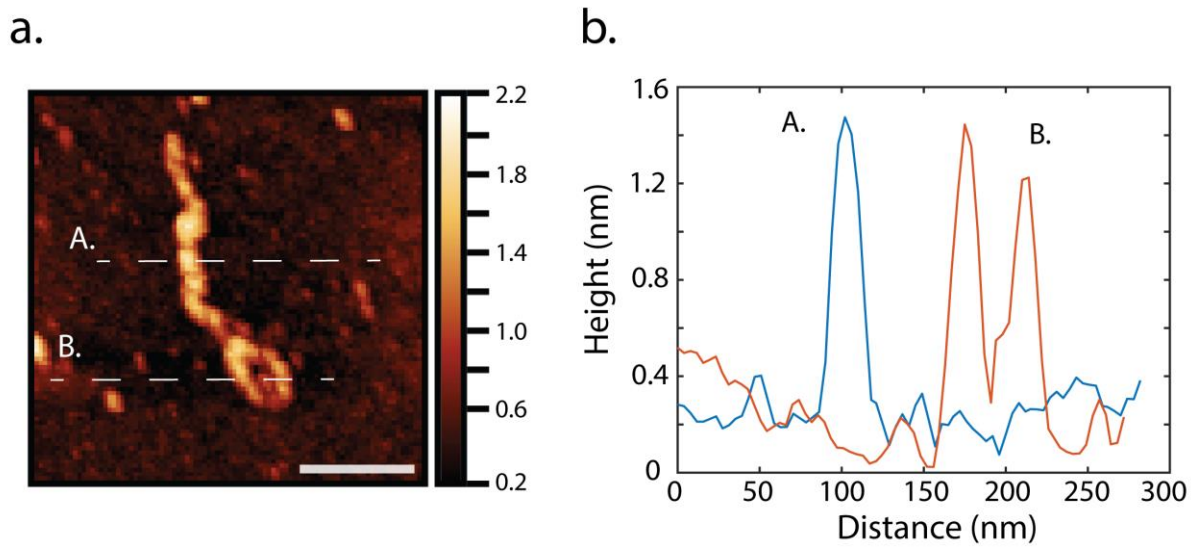

Figure S8. a. Magnified AFM image of linear HH construct bound by H-NS protein. Scale bar 100nm. **b.** Height measurement along the H-NS bound DNA marked by two dotted lines in panel a. The height profiles show that H-NS bridges two DNA duplexes (height profile A) as well as binds to single double strands inside the loop (height profile B). Related to Figure 4.

Supplementary Table 1. Shape parameters of linear nucleoprotein complexes (mean ± sd). Related to Figure 4.

Linear fragment DNA shape parameters					
Sample	**Number**	**$L_{(contour)}$ [nm]**	**$\Delta L_{(contour)}$**	**l_p [nm]**	**R_g [nm]**
Head-Head (HH)					
Control	110	445 ± 25	X	35 ± 5nm	54 ± 13nm
+FIS : kb = 2.6	40	420 ± 30	-6%	27 ± 5nm	42 ± 12nm
+H-NS : kb = 1.06	38	430 ± 30	-3%	43 ± 5nm	52 ± 10nm
+FIS : H-NS : kb = 2.6 : 3.2 : 1	40	390 ± 50	-12%	50 ± 5nm	85 ± 15nm
Head-Tail (HT)					
Control	90	445 ± 30	X	40 ± 5nm	58 ± 15nm
+FIS : kb = 2.6	35	380 ± 45	-15%	27 ± 5nm	51 ± 12nm
+H-NS : kb = 1.06	45	430 ± 30	-3%	40 ± 5nm	55 ± 11nm
+FIS : H-NS : kb = 2.6 : 3.2 : 1	35	460 ± 45	+3%	46 ± 5nm	85 ± 18nm

Transparent Methods

Constructs

The two 3997 bp constructs (Head-to-Tail and Head-to-Head) were constructed as described earlier (Japaridze et al., 2017b). Briefly, the constructs contained sequences with FIS binding sites amplified from the UAS of the *tyrT* gene (denoted as UAS) and sequences with H-NS binding sites amplified from the NRE of *proV* gene (denoted as NRE) of *E. coli*. In these two constructs the individual UAS and NRE elements were cloned in different spatial arrangements.

Protein purification

Native Fis and H-NS were purified as previously described (Lautier and Nasser, 2007, Nasser and Reverchon, 2002). Overproduction of the native Fis and native H-NS were carried out in *E.coli* BL21Δfis/pET20-*fis* and *E.coli* BL21Δhns/pET20-*hns* cells, respectively. Purification of the proteins were achieved from cells grown at 37°C in 3 liters LB medium containing ampicillin (100µg/ml). When the OD_{600nm} reached ~0.5 (for FIS) and ~1.0 (for H-NS), IPTG was added (final concentration of 500µM) and the cells were grown for an additional 1h at 37°C. Cells were pelleted by centrifugation for 10min at 6000 rpm, then washed by buffer A (20mM Tris pH 7.2, 1mM EDTA, 10 % glycerol, 1-4mM DTT, 1mM PMSF, 150mM NaCl) and finally frozen in liquid nitrogen and store at -80°C until purification. All the purification steps were performed at 4°C. Briefly at least 5g of cells were defrosted and suspended in 25ml of buffer A, lysed by 3 steps in French press and then sonicated (10 pulse at 50% of power) to brake DNA and decrease the viscosity of the extract. The obtained mixture was centrifuged 2x at 12000rpm for 30min and the supernatant was diluted 3-fold by buffer A without NaCl to decrease the NaCl final concentration to 50mM. The obtained protein extract was loaded on MonoQ-Hitrap (5ml), wash extensively to remove the unbound material before the elution of the bounded proteins was performed by a linear gradient from 100mM to 800mM NaCl at 3-5 ml/min. After analysis of the obtained fractions on 15% SDS-PAGE, those contained Fis or H-NS were mixed and diluted 3-fold by buffer A without NaCl and loaded to 5ml Heparin (HiTrap, GE healthcare) equilibrated in buffer A containing 50 mM NaCl at 1-2 ml/min. The Heparin column was extensively washed to remove the unbound material before the elution of the bounded proteins by a linear gradient (10-20x the volume of the column at least 50-100ml) from 50mM NaCl to 1.2M NaCl. Elution of Fis and H-NS are observed around

0.5-0.6 M NaCl. After analysis on 15% SDS-PAGE, Fractions containing Fis and H-NS protein of greater than 95% purity, were pooled and dialysed twice for 2h against 2l of storage buffer (20mM Tris-HCl pH7.9, 300mM NaCl, 1mM EDTA, 1mM DTT, 10% glycerol), then overnight against the same buffer containing 40% glycerol. The obtained preparations were stored at −80°C.

Linear DNA sample preparation

Linear DNA fragments were diluted in AFM buffer (20mM Hepes, 50mM KCl, 2mM $NiCl_2$, 0.003% Tween 20, 2.5% Glycerol, pH 7.9) to a final concentration of 10 ng/µl. A control sample, without proteins, was prepared by mixing one microliter of linear fragment DNA with 22 µl of AFM buffer and incubating for 5 min at room temperature on freshly cleaved mica. The mica was then rinsed with 1 ml of ultrapure water and dried under a gentle flow of compressed filtered air.

For protein-DNA constructs first both H-NS and FIS were diluted in the AFM buffer to the desired concentration (FIS - 80 ng/µl, HNS- 22 ng/µl). Several samples at different protein to DNA ratios were then prepared for each construct.

Protein-DNA samples were prepared by mixing 1 µl of protein dilution with 21 µl AFM Buffer and only after mixing the proteins solution well, 1 µl of template DNA (10 ng/µl) was added to the solution. The whole mix (23µl) was incubated for 5 min at 37 °C. As the pre last step, the incubation mix was deposited on freshly cleaved mica surface and incubated at room temperature for 5 min. Finally, the surface was rinsed with 1ml ultrapure water and dried under gentle nitrogen flow.

Circular DNA sample preparation

Circular DNA constructs were nicked using the Nt.BspQI nuclease (New England BioLabs) and purified from 1% agarose gel. DNA was then diluted in the P1 buffer (1mM TRIS-HCl, 4mM MgCl2 , 0.003% Tween 20, 2.5% Glycerol, pH 7.9) to a final concentration of 10 ng/µl. Control samples, without proteins, were prepared by mixing 1 µl of DNA with 22 µl of P1 buffer and incubated for 7 min at room temperature on freshly cleaved mica. The mica was then rinsed with 1 ml of ultrapure water and dried under a gentle flow of compressed filtered air.

Protein-DNA samples were prepared by mixing 1 µl of protein dilution (in P1 Buffer) with 21 µl P1 Buffer and only after mixing the proteins solution well, 1 µl of template DNA (10 ng/µl) was added to the solution. The whole mix (23µl) was incubated for 5 min at 37 °C. As the pre

last step, the incubation mix was deposited on freshly cleaved mica surface and incubated at room temperature for 5 min. Finally, the surface was rinsed with 1ml ultrapure water and dried under gentle nitrogen flow.

AFM imaging

Images were collected using a Multimode atomic force microscope equipped with a Nanoscope IIIa controller (Veeco Instruments, Santa Barbara, CA), operating in Tapping Mode in air using a J-scanner and RTESP silicon cantilevers. All recorded AFM images consist of 512x512 pixels with scan frequencies between 1 and 2 Hz. Each protein-DNA binding experiment was performed at least in duplicate. AFM images were obtained at several separate locations across the mica surface to ensure a high degree of reproducibility and were used for statistical analysis of protein-DNA complexes. Only DNA molecules that were completely visible in AFM image were considered for statistical analysis. AFM images were simply flattened using the Gwyddion software (Version 2.55) without further image processing (Nečas and Klapetek, 2012).

Analysis of AFM images

DNA molecules were trace by using the "DNA Trace" software (Mikhaylov et al., 2013). The tracing step was set between 2.5 and 5nm which corresponds to a size of ~1 pixel (2.5 for linear fragments and 5nm for circular plasmids). Statistics properties such as the contour length and the radius of gyration of DNA molecules (typically between 35–100 individual molecules) were measured using the same "DNA Trace" software. The square of the radius of gyration of a polymer was defined as the sum of the squares of the distances from all monomers to the center of mass, divided by the total number of monomers

$$R^2 = \frac{1}{N}\sum_{i}^{N} r_i^2$$

Where N is the number of monomers in the chain, and r_i is the distance from the i-th monomer to the center of mass (Grosberg and Khokhlov, 1994).

We measured the effective persistence length *lp* of control and protein bound DNA molecules by using the bond correlation function for polymers in two-dimensions,

$$< \cos\theta(s) >= e^{-s/2lp}$$

where θ is the angle between the tangent vectors to the chain at two points separated by the distance *s*, and *lp*, the persistence length (Rubinstein and Colby, 2003). Since the persistence

length of DNA is obtained by treating the molecules assuming their mechanical properties are uniform (and thus ignoring locally bound proteins), we denote it as the effective persistence length. This analysis is a proven method to extract the persistence length for polymer molecules that orient themselves in an unconstrained way at a surface in equilibrium. We apply the approach here as well to nucleoprotein filaments that contain small loops, and denote *lp* as the effective persistence length.

Nanopore experiments

We used TEM-drilled 15 nm diameter SiN nanopores for the experiments. The SiN membrane containing the nanopore was loaded in a PEEK (Polyether ether ketone) flow cell. The DNA samples were diluted in LiCl solution (final conentration 0.9M) to a final concentration of 1ng/µl before being introduced to the cis side (-ve) of the nanopore. We used Ag/AgCl electrodes and an Axopatch 200B amplifier (Molecular Devices) for current detection. In experiments where FIS (5.6ng/µl incubation concentration) and/or H-NS (6ng/µl incubation concentration) were used, the DNA molecules (10ng/µl) were pre-incubated with proteins in 10mM Tris buffer for 10min at room temperature. Afterwards the sample was diluted 10 times into LiCl buffer (final DNA contecntration 1ng/µl in 0.9M LiCl) and added to the cis side of the nanopopore. The traces were recorded at 200 kHz and further low pass filtered at 10 kHz with the Transanalyzer Matlab package (Plesa and Dekker, 2015). As DNA purification quality as well as self-folding of the DNA duplex may affect the current blockade levels, we normalized the blockade levels for each construct to set the control standard for comparison of the protein-bound constructs. To minimize these variations, all sets of measurements were done on the same day with the same batch of DNA and protein preparation as well as on the same nanopore. We set a current blockade threshold at 2.5 times higher than the average current blockade of a single DNA helix event (threshold = $2.5 \cdot I_{DNA}$) and quantified the percentage of events above this threshold as compared to the control. Variation of the thresholding level had nearly no effect on the results, as can be seen in the Supplementary Fig.5k.

SI References

Grosberg, A., and Khokhlov, A. (1994). Statistical Physics of Macromolecules SE - AIP Series in Polymers and Complex Materials (AIP Press).

Lautier, T., and Nasser, W. (2007). The DNA nucleoid-associated protein Fis co-ordinates the expression of the main virulence genes in the phytopathogenic bacterium Erwinia chrysanthemi. Mol. Microbiol. 66, 1474–1490.

Japaridze, A., Renevey, S., Sobetzko, P., Stoliar, L., Nasser, W., Dietler, G., and Muskhelishvili, G. (2017b). Spatial organization of DNA sequences directs the assembly of bacterial chromatin by a nucleoid-associated protein. J. Biol. Chem. 292, 7607–7618.

Mikhaylov, A., Sekatskii, S.K., and Dietler, G. (2013). DNA trace: a comprehensive software for polymer image processing. J. Adv. Microsc. Res. 8, 241–245.

Nasser, W., and Reverchon, S. (2002). H-NS dependent activation of pectate lyases synthesis in the phytopathogenic bacterium Erwinia chrysanthemi is mediated by the PecT repressor Mol. Microbiol. 43, 733–748.

Necas, D., and Klapetek, P. (2012). Gwyddion: an open-source software for SPM data analysis. Cent. Eur. J. Phys. 10, 181–188.

Plesa, C., and Dekker, C. (2015). Data analysis methods for solid-state nanopores. Nanotechnology 26, 084003.

Rubinstein, M., and Colby, R.H. (2003). Polymers Physics (Oxford University Press).